HHS Public Access

Author manuscript

Nat Cancer. Author manuscript; available in PMC 2022 February 16.

Published in final edited form as:

Nat Cancer. 2021 September ; 2(9): 932–949. doi:10.1038/s43018-021-00238-0.

Targeting PUS7 suppresses tRNA pseudouridylation and glioblastoma tumorigenesis

Qi Cui[1,8], **Kailin Yin**[2,8], **Xiaoting Zhang**[2,8], **Peng Ye**[1], **Xianwei Chen**[1], **Jianfei Chao**[1], **Haowei Meng**[2], **Jiangbo Wei**[3], **Roeth Daniel**[4], **Li Li**[1], **Yue Qin**[1], **Guihua Sun**[5], **Mingzi Zhang**[1], **Jeremy Klein**[1], **Marvin Huynhle**[1], **Cheng Wang**[1], **Leying Zhang**[6], **Behnam Badie**[6], **Markus Kalkum**[4], **Chuan He**[3], **Chengqi Yi**[2,*], **Yanhong Shi**[1,7,*]

[1]Division of Stem Cell Biology Research, Department of Developmental and Stem Cell Biology, Beckman Research Institute of City of Hope, Duarte, CA, 91010.

[2]State Key Laboratory of Protein and Plant Gene Research, School of Life Sciences; Peking-Tsinghua Center for Life Sciences, Peking University, Beijing, China.

[3]Department of Chemistry and Department of Biochemistry and Molecular Biology, and Institute for Biophysical Dynamics, Howard Hughes Medical Institute, The University of Chicago, 929 East 57th Street, Chicago, IL 60637, USA.

[4]Department of Molecular Imaging and Therapy, Beckman Research Institute of City of Hope, Duarte, CA, 91010.

[5]Diabetes and Metabolism Research Institute at City of Hope, Duarte, CA, 91010.

[6]Department of Surgery, Beckman Research Institute of City of Hope, Duarte, CA, 91010.

[7]Irell & Manella Graduate School of Biological Sciences, Beckman Research Institute of City of Hope, Duarte, CA, 91010.

[8]These authors contributed equally.

[*]Correspondence to Y. C. chengqi.yi@pku.edu.cn and Y.S. yshi@coh.org.

Author Contributions

Y.S., C.Y., Q.C., K.Y. and X.Z. designed experiments and interpreted results. Q.C. performed experiments. K.Y. performed small RNA DM-Ψ-seq and pseudouridine seq experiments from cells provided by Q.C.. X.Z., H.M., and K.Y. performed DM-Ψ-seq, pseudouridine seq, and TYK2 codon usage analysis. Q.C. performed luciferase reporter assay using reporter constructs prepared by K.Y.. Y.S., C. H., J.W. and Q.C. designed the polysome profiling experiment. J.W. performed polysome profiling analysis from cells provided by Q.C.. Y.S., M.K., Q.C., and R.D. designed the TMT proteomics experiment. R.D. performed the TMT proteomics experiment from cells provided by Q.C. P.Y. and Q.C. performed PBT003 cell transplantation experiment and PUS7 inhibitor in vivo treatment experiments. X.C. established and performed in vitro PUS7 activity assay with substrates designed and prepared by Q.C. and MS sample injection by J.C.. J.C. helped with MS analysis of PUS7 inhibitor-treated samples provided by Q.C.. L.L. prepared sgRNA construct and performed Western blot for TYK2 and STAT1. Q.C. prepared samples for RNA-seq analysis in the Integrative Genomics Core. X.Z. and Q.C. performed PUS7 and ISG correlation analysis. L.Z. and B.B. provided GBM patient tissues and established GBM cell lines. G.S. designed PUS7 shRNA constructs and prepared CDS of PUS7 constructs. Y.Q. performed OP-puro incorporation assay and cell cycle analysis from cells provided by Q.C.. M.Z. performed TMA IHC analysis and apoptosis analysis. K.Y. performed nascent protein synthesis assay and protein silver staining. J.K. provided technique help with PBT707 transplantation and tumor imaging. M.H. performed Western blot for PUS7 in GSC and NSC samples provided by Q.C., M.Z. and C.W. provided astrocytes. Y.S., C.Y., Q.C., K.Y. and X.Z. wrote the manuscript with comments from all other authors.

Conflict of interest statement

C. H is a scientific founder and a member of the scientific advisory board of Accent Therapeutics Inc. The other authors declare no conflict of interest.

Abstract

Pseudouridine is the most frequent epitranscriptomic modification. However, its cellular functions remain largely unknown. Here we show that the pseudouridine synthase PUS7 is highly expressed in glioblastoma versus normal brain tissues, and high PUS7 expression levels are associated with worse survival in glioblastoma patients. The PUS7 expression and catalytic activity are required for glioblastoma stem cell (GSC) tumorigenesis. Mechanistically, we identified PUS7 targets in GSCs through small RNA pseudouridine sequencing, and showed that pseudouridylation of PUS7-regulated tRNA is critical for codon-specific translational control of key regulators of GSCs. Moreover, we identified chemical inhibitors for PUS7, and showed that these compounds prevented PUS7-mediated pseudouridine modification, suppressed tumorigenesis, and extended lifespan of tumor-bearing mice. Overall, we identified an epitranscriptomic regulatory mechanism in glioblastoma and provided preclinical evidence of a potential therapeutic strategy for glioblastoma.

Keywords

RNA modification; epitranscriptomics; pseudouridylation; translational control; glioblastoma; glioblastoma stem cells

Introduction

Over 100 types of posttranscriptional modifications have been discovered in RNA[1]. Increasing studies have demonstrated that RNA modifications are critical in epigenetic regulation of gene expression in physiology and disease[2]. Pseudouridine (Ψ), an isomer of uridine, is the most abundant RNA modification[3,4], therefore called “the fifth RNA nucleotide”[5]. The isomerization of uridine to pseudouridine can be catalyzed by either snoRNA-dependent mechanism that requires the box H/ACA ribonucleoproteins or RNA-independent mechanism that involves the stand-alone pseudouridine synthase (PUS) enzymes[6]. These PUS enzymes are divided into six families, including TruA, TruB, TruD, RsuA, RluA, and Pus10 family[7,8], among which, PUS7 is the only member of the TruD family[9].

Pseudouridine mainly occurs in noncoding RNAs, such as rRNAs (ribosomal RNAs), tRNAs (transfer RNAs), and snRNAs (small nuclear RNAs), and also in pre-mRNAs, and contributes to critical biological processes such as translation and mRNA splicing[8]. With the advance of high-throughput sequencing, recently developed pseudouridine sequencing technologies (Ψ-seq, Pseudo-seq, CeU-seq, Psi-seq and DM-Ψ-seq) revealed prevalent pseudouridine modification in not only tRNA, rRNA, and snRNA, but also mRNA, where it can be dynamic under stress conditions[10–15]. While RNA pseudouridylation has been implicated in human physiology and diseases[9,16,17], the biological roles of PUSs remain largely undefined.

Glioblastoma multiforme (GBM) is the most common and aggressive primary brain tumor in adults. However, current treatments are only palliative. Despite great efforts in therapeutic development, median survival of GBM patients remains less than 16 months

after diagnosis[18,19]. It is believed that glioblastoma stem cells (GSCs) are important for GBM tumor progression and treatment resistance[20–25]. Although the role of m^6A RNA modification in glioblastoma is starting to be revealed[26–29], whether and how other RNA modification machinery impacts GBM tumorigenesis remains largely unexplored. Pseudouridine is the most abundant RNA modification and increased levels of pseudouridine has been detected in cancer patients[30,31]. However, the biological roles of pseudouridine modification and PUS enzymes remain largely undefined in cancer and especially in GBM.

Our analysis of PUS enzymes in GBM revealed statistically significant association between PUS expression and GBM patient median survival in GBM datasets. Such association prompted us to explore the role of PUS7 in GBM tumorigenesis. By manipulating PUS7 expression in GSCs through gene knockdown, knockout and overexpression, we demonstrated that PUS7 plays an important role in GBM tumorigenesis. Through RNA, protein and pseudouridine profiling, we showed that PUS7 controls GSC growth through codon-specific translational control of key regulators of GSCs via PUS7-dependent tRNA modification. We also identified chemical inhibitors of PUS7 in this study and determined the effect of these chemicals in GSC growth and tumorgenicity.

Results

High PUS7 expression in GBM patients predicts poor prognosis

As the most abundant RNA modification, while RNA pseudouridylation has been implied in human physiology and diseases, the biological roles of PUS remain largely undefined in cancer and especially GBM. To reveal the functional relevance of PUS enzymes in GBM, we examined the expression of PUS in the Chinese Glioma Genome Atlas (CGGA) database[32], the Repository for Molecular Brain Neoplastic Data (REMBRANDT) database[33], the Cancer Genome Atlas (TCGA) database[34], and the Gravendeel dataset[35]. Among all the PUS enzymes, the expression of PUS7 is most strongly associated with the progression of GBM. PUS7 is the only PUS that exhibits statistically significant association between PUS expression and GBM patient median survival in three out of four datasets examined, with $p=0.0039$ in the CGGA database, $p= 0.0345$ in the REMBRANDT database, and $p= 0.0161$ in the Gravendeel dataset (Supplemental table 1). Upregulated expression of PUS7 predicts worse survival in GBM patients (Supplemental table 1). Although the association did not reach statistical significance in TCGA, the same trend of association between higher PUS7 expression and worse GBM patient medium survival was observed as in the other databases we analyzed. The expression level of PUS7 is much higher in GBM patients than that in non-tumor control subjects (Figures 1A and supplemental table 2). Moreover, we found that the PUS7 expression level is associated with the IDH status in all glioma patients but not GBM only patients, with low expression of PUS7 in glioma patients that have IDH mutation, which are often associated with better patient survival[36,37] (Figure 1B, Extended Data Figure 1A, and 1B). After excluding IDH mutant patients from GBM patients, there is still a statistically significant association between higher PUS7 expression and worse patient median survival in GBM patients in the CGGA and Rembrandt datasets (Extended Data Figure 1C and 1D). Although the association did not reach statistical significance in TCGA and Gravendeel datasets, the same trend

of association between higher PUS7 expression and worse GBM patient medium survival was observed in these datasets (Extended Data Figure 1E and 1F). In addition, there is a statistically significant association of PUS7 expression with gain of chromosome 7 and loss of chromosome 10 status. Increased PUS7 expression is associated with gain of PUS7 copy number variations, but not gain of chromosome 19/20 status in GBM patients (Figure 1C), indicating a correlation between PUS7 expression and chromosome abnormality in GBM.

Consistent with increased PUS7 mRNA expression in GBM patients as shown in the datasets (Figure 1A), the protein level of PUS7 is elevated considerably in GBM patient tissues, compared to non-tumor control tissues, as revealed by Western blot (Figure 1D and 1F) and immunohistochemistry (IHC) analysis of GBM tissue microarray (Extended Data Figure 1G and 1H). A portion (32.86%) of PUS7-positive cells in GBM tissues also expressed the GSC marker SOX2 (Extended Data Figure 1G), suggesting that these cells could be GSCs. The remaining PUS7-positive cells could include cells expressing other GSC markers[38–45] or differentiated cells that express lower level of PUS7.

Although both patient-derived GSCs and control brain-derived normal NSCs share the self-renewal ability, only GSCs can give rise to tumors. While intensive studies have investigated the tumor-initiating/propagating properties of GSCs, what distinguishes GSCs and NSCs remains a topic of interest in order to develop drugs that specifically targets GSCs. We found that the protein expression level of PUS7 was substantially higher in GSCs than that in NSCs and human astrocytes (Figure 1E and 1G). The expression of PUS7 in established GBM cells varied among different lines (Figure 1E). One possible reason is that these established GBM cell lines have different extent enrichment of cancer stem-like cells[46]. Taken together, the elevated expression of PUS7 in GBM tissues and GSCs suggests that PUS7 may play a role in GBM tumorigenesis.

PUS7 regulates GSC growth and self-renewal

To study the role of PUS7 in GSC growth and self-renewal, we knocked down PUS7 in multiple lines of GSCs derived from different GBM subtypes[20], including classical, mesenchymal, and proneural. Knockdown (KD) of PUS7 was confirmed by RT-PCR (Extended Data Figure 2A) and Western blot (Extended Data Figure 2B). The growth of all six GSC lines was dramatically suppressed after KD of PUS7 (Figure 2A and Extended Data Figure 2C). KD of PUS7 also inhibited the self-renewal of GSCs as revealed by reduced sphere formation rate (Figure 2B and Extended Data Figure 2D) and decreased stem cell frequency (Figure 2C) in PUS7 KD GSCs. To corroborate the effect of shRNA-mediated KD, we knocked out PUS7 in PBT003 GSCs by CRISPR/Cas9 editing using two independent sgRNAs. Western blot revealed substantially reduced PUS7 protein level by both sgRNAs in PUS7 knockout (KO) PBT003 GSCs (Extended Data Figure 2E). The growth and self-renewal of GSCs were inhibited by PUS7 sgRNAs, compared to control sgRNA (Extended Data Figure 2F and 2G). Consistently, PUS7 KO led to increased cell cycle arrest in G0/G1 phase (Extended Data Figure 2I). No statistically significant increase in cell apoptosis was detected in PUS7 KO PBT003 GSCs as revealed by active caspase 3 staining (Extended Data Figure 2H). Taken together, these data indicate that PUS7 plays an important role in GSC growth and self-renewal.

After demonstrating that PUS7 is necessary for GSC growth and self-renewal by KD/KO, we next tested whether PUS7 is sufficient to promote GSC growth and self-renewal by overexpressing PUS7 in GSCs. A mutant PUS7 (D256A) with abolished enzymatic activity was included as a control[47]. Overexpression of the wild type (WT) PUS7 and the catalytically inactive D256A mutant was confirmed by Western blot (Extended Data Figure 2J). The growth of GSCs with overexpression of the WT PUS7 was increased, compared to control GSCs transduced with an empty vector (Figure 2D). In contrast, overexpression of the catalytically inactive PUS7 D256A mutant failed to promote GSC growth. Moreover, overexpression of the WT, but not the D256A mutant PUS7, rescued the growth defects induced by PUS7 KD in GSCs (Extended Data Figure 3). The self-renewal capacity of GSCs, as revealed by sphere formation rate (Figure 2E) and stem cell frequency (Figure 2F), was also increased in GSCs with overexpression of the WT but not the mutant PUS7, compared to control cells. These results together indicate that PUS7 promotes the growth and self-renewal of GSCs in an enzymatic activity-dependent manner.

Reduced PUS7 expression in GSCs suppresses tumor progression

To study whether KD of PUS7 affects GSC tumorigenicity *in vivo*, we transplanted GSCs with or without KD of PUS7 into immunodeficient NSG mice. Tumor growth was monitored by bioluminescent imaging (Figure 3A and 3D). Tumor progression was dramatically inhibited in NSG mice transplanted with PUS7 KD GSCs, compared to control mice (Figure 3B, 3C and 3E, 3F). Moreover, NSG mice transplanted with PUS7 KD GSCs survived substantially longer, compared to control mice (Figure 3G and 3H).

To corroborate the effect of shRNA-mediated KD of PUS7 on GSC tumorigenicity, we transplanted GSCs with sgRNA-mediated PUS7 KO into NSG mice. Similar to shRNA-mediated KD, sgRNA-mediated PUS7 KO also inhibited GSC-derived tumor growth dramatically (Extended Data Figure 4A and 4B). Accordingly, NSG mice transplanted with PUS7 KO GSCs survived much longer than the control mice (Extended Data Figure 4C). Moreover, the inhibitory effect on tumor progression by PUS7 KO could be rescued by overexpression of the WT, but not the catalytically mutant PUS7 in GSCs (Figure 3I and 3J). This result indicates that PUS7 regulates GSC tumorigenicity in an activity-dependent manner. Taken together, these results demonstrate that reduced PUS7 expression suppresses GSC tumorigenicity and prolongs the life span of GSC-derived tumor-bearing mice.

PUS7 inhibitors suppress GSC growth

Inspired by the robust tumor-inhibitory effect of PUS7 KD/KO, we identified small molecule inhibitors of PUS7 in order to modulate PUS7 in a pharmacologically relevant manner. We screened 270,000 NCI-DTP compounds and 4,086 FDA-approved drugs in a virtual screening to identify small molecules that are predicted to alter PUS7 enzymatic activity. To identify “hits” from the virtual screen candidates, we established an *in vitro* enzymatic assay as secondary screen using recombinant PUS7 and a synthetic RNA substrate for pseudouridine modification. Pseudouridine level in the RNA substrate was increased by PUS7 protein (positive control, PC), compared to the negative control (NC) that has no PUS7 protein. Treatment with compounds from the initial screen led to altered pseudouridine level catalyzed by PUS7 recombinant protein, as revealed by a change in the

Ψ to U ratio. Among compounds that reduced PUS7 activity, compounds 4 (C4) and 17 (C17) exhibited the strongest inhibitory effect (Figure 4A). To determine the cellular effect of these compounds, we treated PBT003 GSCs with C4 and C17 at doses from 0.4 μM to 50 μM. Compound C4 exhibited dose-dependent inhibition of PBT003 growth, but mildly (Extended Data Figure 5A), compound C17 strongly suppressed the growth of PBT003 at the concentrations tested (Figure 4B).

Intrigued by the strong growth-inhibitory effect of compound 17, we tested the effect of C17 at nM concentrations and observed dose-dependent inhibition of PBT003 growth by C17 from 4 nM to 400 nM. The IC50 of C17 was 92.15 nM in PBT003 cells (Figure 4C and Extended Data Figure 5B and 5C). The same dose-dependent growth-inhibitory effect by C17 was observed in other GSC lines, including PBT707, PBT726 and PBT111 cells (Figure 4C and Extended Data Figure 5C). In contrast, there is no inhibitory effect on control NSCs by C17 at 100 nM or lower concentrations (0–40 nM), and much less effect (compared to GSCs) at 400 nM of C17 (Figure 4C, 4D, and Extended Data Figure 5B). These results indicate that compound C17 inhibits the growth of GSCs in a dose-dependent manner and that it preferentially targets GSCs compared to NSCs.

We next test if the cellular effect of C17 is dependent on PUS7. We showed that C17 was able to reduce the growth of the WT but not PUS7 KO PBT707 GSCs (Figure 4E), suggesting that this compound could act through PUS7. Moreover, we found that overexpression of the WT but not the catalytically mutant PUS7 was able to rescue the growth-inhibitory effect of C17 in PBT707 GSCs (Figure 4F). Taken together, these results indicate that C17 regulates GSC growth in a PUS7-dependent manner.

We identified a structural analog of C17 and showed that the analog could also inhibit GSC growth in a dose-dependent manner (Figure 4G and Extended Data Figure 5D). Consistent with inhibition of PUS7-dependent pseudouridine modification by C17 *in vitro*, we observed a substantial decrease in pseudouridine level in GSCs treated with C17 or its analog (Figure 4H and 4I). Taken together, these data demonstrate that compound C17 and its structural analog could inhibit pseudouridine modification by PUS7 and suppress GSC growth.

The PUS7 inhibitor C17 suppresses tumor progression *in vivo*

To test the effect of inhibition of pseudouridine modification in a preclinical model, we treated GSC-derived tumor-bearing NSG mice with the C17 compound. Specifically, PBT003 GSCs expressing a luciferase reporter were transplanted into NSG mice to establish tumors, followed by compound treatment at 5 μl of 400 nM C17 (Figure 5A), corresponding to 25.9 ng/Kg C17 for a 25 g mouse, which could allow achievement of a dose close to the IC50 dose of 92.15 nM, based on our preliminary pharmacodynamics study that detected an average of about 1/5 of the initial dose 3 h after C17 injection. The growth of GSC-derived tumors was significantly inhibited by the treatment of C17, compared to the treatment with vehicle control (Figure 5B and 5D). Accordingly, decreased pseudouridine level was detected in tumor tissues treated by C17 (Figure 5C), confirming the inhibition of PUS activity by C17 in vivo. Moreover, the survival of NSG mice treated with C17 was dramatically prolonged, compared to vehicle treated mice (Figure 5E). A similar tumor-inhibitory effect by C17 was detected in PBT707 GSC-transplanted NSG mice (Figure

5F-I). Taken together, these results indicate that inhibition of PUS7 activity could suppress GSC-derived tumor progression and prolong the lifespan of tumor-bearing mice.

PUS7 regulates tRNA pseudouridylation and translation in GSC

Having uncovered an important role for PUS7 in regulating GSC growth and tumorigenicity, we next determined how PUS7 exerts this function. We detected PUS7-regulated pseudouridine modification in GSCs through mass spectrometry and DM-Ψ-seq, a recently developed pseudouridine sequencing method for small RNA[14]. RNAs were prepared from control and PUS7 KO PBT003 GSCs, fractionated into small RNA (<200 nt) and >200 nt RNAs, and subjected to mass spectrometry analysis. We detected a significant decrease in pseudouridine level in the small RNA population in PUS7 KO GSCs, compared to that in control cells (Figure 6A), whereas no considerable change was observed in >200 nt RNAs of the PUS7 KO GSCs (Figure 6A).

To identify the pseudouridine modification profile in small RNAs, control and PUS7 KO PBT003 GSCs were subjected to small RNA DM-Ψ-seq. We detected 824 pseudouridine sites in tRNA (Figure 6B and Supplemental table 3) and 6 sites in snRNA (Supplemental table 3). By comparing the Ψ profiles between control and PUS7 KO PBT003 GSCs, we identified 13 PUS7-dependent pseudouridine sites in 8 tRNA types (Supplemental table 4), and no PUS7-dependent pseudouridine sites in snRNAs. In addition to PUS7-regulated pseudouridine sites at positions 13 and 35 of tRNA as reported in previous studies[34], we identified pseudouridine sites at the 50th position of several tRNA isoforms. For instance, tRNA-Arg-CCG-2–1 at position 50 exhibited a dramatic decrease in pseudouridine modification upon PUS7 KO in GSCs (Figure 6C, 6D and Extended Data Figure 6A). The DM-Ψ-seq data were verified using primer extension (Extended Data Figure 6B). The DM-Ψ-seq and primer extension data together indicate that position 50 in tRNA-Arg-CCG-2–1 is a true Ψ modification site and this modification is PUS7-dependent. In addition, we detected a decrease of pseudouridylation level by C17 treatment in tRNAs with PUS7-dependent Ψ sites, such as tRNA-Val-AAC-3–1 and tRNA-Glu-TTC-4–1 (Extended Data Figure 6C and Supplemental table 6). In contrast, the Ψ sites in rRNA were unperturbed by C17 treatment (Supplemental table 8).

In addition to GSCs, we performed small RNA DM-Ψ-seq in NSCs to compare the pseudouridine modification profiles in GSCs vs NSCs. Although most Ψ sites were shared by GSCs and NSCs (Figure 6E and Supplemental table 5), a list of GSC-specific Ψ sites was identified (Supplemental table 5). In GSC-specific pseudouridine sites, we found that tRNA-Arg-CCG-2–1, which was identified as a tRNA with PUS7-dependent pseudouridine site at position 50, showed a clear increase in pseudouridylation level at position 50 in GSCs compared to NSCs (Figure 6F and Supplemental table 5). This result suggests that PUS7 could induce cell type-specific tRNA pseudouridylation in GSCs vs NSCs to regulate GBM tumorigenesis.

To test whether loss of PUS7-mediated modification affects the stability of target tRNAs, we analyzed tRNA levels in control and PUS7 KO GSCs using input samples in small RNA DM-Ψ-seq. The global tRNA level was not changed in PUS7 KO cells, compared to control cells (Extended Data Figure 6D and Supplemental table 7). Northern blot confirmed that

KO of PUS7 did not affect the level of tRNAs, such as tRNA-Arg-CCG, that contains PUS7-dependent Ψ sites (Extended Data Figure 6E). In addition, we performed tRNA-derived fragment (tRF) analysis and detected no significant change in the level of tRFs derived from tRNAs that have PUS7-dependent Ψ sites in PUS7 KO PBT003 GSCs (Extended Data Figure 6F and Supplemental table 7).

A previous study showed that PUS7 can globally repress translation in human embryonic stem cells and hematopoietic stem cells[16], we tested if PUS7 could similarly regulate global translation in GSCs. Puromycin incorporation analysis using OPP (O-propargyl-puromycin, an alkyne analog of puromycin) was performed to test global translation in GSC. The OP-puro incorporation analysis revealed no obvious change in global translation in PUS7 KO PBT003 GSCs (Extended Data Fig. 6G). Similarly, nascent protein synthesis analysis revealed no obvious change in global translation in PUS7 KO HEK293T cells (Extended Data Figure 6H).

We next tested if PUS7 could regulate translation in a more specific manner via its target tRNAs in GSCs. A dual luciferase reporter system was used to test the translation of tRNAs by fusing 6 x codons with the firefly luciferase. While the global translation efficiency revealed by the control reporter was not changed upon KO of PUS7 in PBT003 (Figure 6G), the translation efficiency of a PUS7-regulated tRNA-Arg-CCG, but not a control tRNA-Arg-TCG, was significantly increased in PUS7 KO GSCs (Figure 6G and Extended Data Figure 6I). The increased translation efficiency of PUS7-regulated tRNA-Arg-CCG in PUS7 KO GSCs was reversed by overexpression of the WT but not the catalytically inactive mutant PUS7 (Figure 6H). These results indicate that PUS7-mediated pseudouridylation in tRNA inhibits codon-specific translation in GSCs.

In addition to small RNAs, we performed transcriptome-wide Ψ sequencing in mRNAs and rRNAs. In rRNA, 89 previously reported[48] Ψ sites were identified in both control and PUS7 KO PBT003 GSCs with similar extent of modification (Supplemental table 8), suggesting that these sites are likely not PUS7-dependent. In mRNAs, 155 Ψ sites were identified in PBT003 GSCs, 13 of which were PUS7-dependent (Supplemental table 9, it is worth noting that some Ψ sites may be missed due to the stringent cutoff criteria or redundancy). It was reported that the consensus Ψ motif for PUS7 was UGΨAR (R=A/G)[16]. Consistently, we identified the motif UGΨAG for PUS7-dependent sites in mRNAs of PBT003 GSCs (Figure 7A). These sites are located on both coding and non-coding RNAs (Figure 7B and Supplemental table 9).

PUS7 regulates GSC growth through TYK2-mediated IFN pathway

To investigate PUS7-regulated pathways, RNAs were prepared from control or PUS7 KO PBT003 GSCs and subjected to RNA-seq. Whole transcriptome analysis revealed 205 up-regulated and 46 down-regulated genes in PUS7 KO GSCs compared to control GSCs. Among the differentially expressed genes (>1.5-fold), the interferon (IFN) pathway is the top GO-term that is regulated by PUS7 KO. 80 out of 205 up-regulated genes were IFN-stimulated genes (ISGs), including CXCL10, IFIT1, ISG15, XAF1, MX1, and OAS1 (Figure 7C, 7D and Supplemental table 9). Up-regulation of ISGs can be reversed by overexpressing the WT but not the mutant PUS7 in PUS7 KO GSCs (Figure 7E). In

addition, we found an inverse correlation between PUS7 expression and ISG expression in GBM patients in the TCGA dataset (Figure 7F, Extended Data Figure 7A and Supplemental table 9), supporting the regulation of ISG expression by PUS7. IFN treatment also reduced GSC growth (Extended Data Figure 7B), consistent with the growth inhibitory effect of PUS7 KD (Figure 2A and Extended Data Figure 2A). In addition, we observed up-regulation of ISG expression by C17 in PBT003 GSCs *in vitro* (Extended Data Figure 7C) and PBT003-derived tumors *in vivo* (Extended Data Figure 7D), indicating that C17 inhibition could affect this pathway.

How does PUS7 regulate the IFN pathway? RNA-seq was not able to provide a clue. We did not detect pseudouridine modification sites in ISG mRNAs or obvious mRNA level change in mRNAs with PUS7-dependent Ψ sites in PUS7 KO PBT003 GSCs either (Supplemental table 9). Thus, we hypothesized that PUS7 may control protein expression to regulate the IFN pathway. We performed quantitative proteomics using the tandem mass tag (TMT) system in control and PUS7 KO PBT003 GSCs. A significant change in the expression of 189 genes was detected at the protein level (Supplemental table 10). Consistent with reduced growth and self-renewal of PUS7 KO GSCs, we observed decreased protein expression of a list of oncogenes and increased protein expression of tumor suppressors in GSCs upon PUS7 KO. Among the list, tyrosine kinase 2 (TYK2), an important regulator of the IFN pathway, was upregulated at the protein level (Figure 8A and 8B) but not mRNA level (Figure 8C) in PUS7 KO GSCs, suggesting that PUS7 may regulate TYK2 protein synthesis. The upregulation of TYK2 protein expression in PUS7 KO GSCs was confirmed by Western blot (Figure 8D). Consistent with increased TYK2 expression, the phosphorylated STAT1, a downstream effector of TYK2, was increased in PUS7 KO GSCs, while the total STAT1 level was not changed (Figure 8E).

We then asked whether PUS7-mediated tRNA pseudouridylation could regulate TYK2 protein expression. Codon usage analysis revealed that codon usage of the PUS7-regulated tRNA-Arg-CCG is 2.6% in TYK2, higher than 90% of genes (Figure 8F), whereas tRNA-Arg-CGA, which is not a PUS7 target in GSCs, is much less used in TYK2 (0.67%) (Figure 8F). Among the 189 differentially expressed proteins identified by the TMT analysis, we found 17 of 94 up-regulated proteins had high usage of codons for tRNA-Arg-CCG (codon usage frequency >2%, rank >80%) (Supplemental table 10). This ratio is significantly (one-sample t-test, two-tailed p-value =1.292e-08) higher than a background level (Supplemental table 10). In addition, we expanded our codon bias analysis for TYK2 to other tRNA substrates of PUS7 and found that 5 of 8 PUS7-dependent tRNAs in GSCs are frequently used in TYK2, including tRNA-Arg-CCG, tRNA-Gln-CTG, tRNA-Asp-GTC, tRNA-Glu-CTC and tRNA-Tyr-GTA (Supplemental table 10). These results suggest that PUS7 may play a role in modulating TYK2 translation through PUS7-modified tRNAs. Accordingly, polysome profiling analysis revealed that the occupancy of polysomes on TYK2 mRNA was substantially elevated in PUS7 KO GSCs (Figure 8G), supporting a role for PUS7 in regulating TYK2 translation. To further support this idea, we mutated the CGG codon of Arg to the CGA codon of Arg in a Flag-tagged TYK2 fragment. The CGG codon corresponds to the PUS7-regulated tRNA-Arg-CCG, whereas the CGA codon corresponds to the PUS7-independent tRNA-Arg-TCG. PUS7 KO in GSCs led to increased protein expression of the WT Flag-TYK2, but not that of the mutant TYK2, in which the CGG

codons were mutated to the CGA codons (Figure 8H, Extended Data Figure 8A, 8B and 8C). These data indicate that PUS7 regulates the expression of TYK2 at the translation level via tRNA pseudouridylation.

We next investigated whether PUS7 regulates GSC growth by modulating the TYK2 pathway. TYK2 KO increased the growth of GSCs (Figure 8I and Extended Data Figure 8D), consistent with increased GSC growth upon STAT1 KO (Figure 8I and Extended Data Figure 8E). More importantly, KO of either TYK2 or STAT1 rescued reduced GSC growth induced by KO of PUS7 (Figure 8J and Extended Data Figure 8F). Treatment of GSCs by a STAT1 inhibitor fludarabine also rescued the growth inhibition by PUS7 KO in GSCs (Extended Data Figure 8G). Taken together, these data indicate that PUS7 could regulate GSC growth by modulating the TYK2-STAT1 pathway.

Discussion

Pseudouridine is the most abundant modification in RNA, but its biological functions in physiology and diseases are not well known. In this study, we demonstrate that the pseudouridine synthase PUS7 is highly expressed in GSCs and regulates GBM tumorigenesis. Patient database and tissue analysis revealed that the PUS7 expression level is significantly higher in GBM patients than that in non-tumor population and that elevated PUS7 expression level is correlated with poor prognosis of GBM patients. Consistent with patient data, substantially higher expression level of PUS7 was detected in GBM patient brain-derived GSCs than control NSCs. KD of PUS7 dramatically suppresses GSC growth, self-renewal and tumorigenesis. In contrast, overexpression of PUS7 promotes the growth and self-renewal of GSCs. Mechanistically, PUS7 regulates GSC growth through codon-specific translational control of key regulators of GSCs. Moreover, pharmacologically targeting PUS7-mediated pseudouridylation efficiently suppresses GSC-derived tumor progression, suggesting that targeting the epitranscriptomic pseudouridine modification could be a promising strategy for anti-GBM therapy.

The study of RNA modification in cancer is a fast-growing field. It has been shown that there is higher urinary pseudouridine nucleoside level in cancer patients[30] and urinary pseudouridine level may serve as a potential tumor marker[49]. In addition, increased levels of pseudouridine nucleosides are detected in prostate cancer[31]. However, a direct role of pseudouridine modification and the PUS enzymes in cancer has not been established. A recent study suggests a potential role for PUS7 in myelodysplastic syndromes (MDS)[16]; yet the cause-effect relationship between PUS7 and MDS pathogenesis remains to be determined. In this study, we have uncovered a direct role of PUS7 in GBM tumorigenesis. We demonstrate that PUS7 regulates the growth and tumorigenesis of GSCs through modulating TYK2 translation via PUS7-dependent tRNA pseudouridylation, providing a direct evidence for PUS7 in modulating tumorigenesis.

RNA modifications play a critical role in controlling RNA functions and regulating gene expression[50]. As a critical component of translation machinery, tRNA is processed and matured with multiple types of modifications. These modifications affect translation through various aspects, including translation rate, tRNA-derived fragment biogenesis, and

codon optimization[50]. In this study, we show that PUS7-mediated pseudouridine in tRNA affects its translation efficiency, in turn regulating downstream gene expression and GBM tumorigenesis.

Pseudouridine has been detected in most RNA species owing to advances in next-generation sequencing techniques[51]; yet the functions of this epitranscriptomic mark are just starting to be revealed. For instance, PUS7-mediated pseudouridylation has been associated with intellectual disability[52–54]. Recently, it has been shown that PUS7-governed pseudouridylation of tRNA-derived fragments controls global translation in embryonic and hematopoietic stem cells[16]. In this study, neither did we detect pseudouridine modification at the 8th position of tRNA, nor did we observe a global translation change mediated by PUS7 in glioblastoma cells. This discrepancy could be due to a difference between the biological systems. PUS7 may function differently in cancer cells from normal cells. Instead of global translation modulation, we show that PUS7 regulates protein synthesis of a subset of genes via its tRNA targets, for instance TYK2, the translation of which is highly dependent on PUS7-modified tRNAs. The detailed mechanism of how PUS7-regulated tRNA controls TYK2 expression remains to be further investigated. It would also be interesting to find out whether PUS7-regulated tRNA controls the expression of other important regulators besides TYK2 to impact development and disease in the future.

IFN-mediated anti-tumor effect and immune regulation play a critical role in cancer progression and cancer therapeutic development. Despite the well-established anti-tumor effect of IFN, there are different views of the pathological role for IFN pathway in glioma. Although one study detected constitutive phosphorylation of STAT1 in glioma cells[55], other studies showed that components of the IFN signaling pathway were downregulated in GSCs, compared to non-stem tumor cells or differentiated glioma cells[56–58]. For example, Zhan et al showed that the expression of STAT1 is reduced in GSC and the low expression of STAT1 is critical for GSC proliferation[56]. Of interest, a recent study showed that in glioblastoma patients, the expression of ISGs is negatively correlated with the expression of SOX2, a core regulator of GSCs that mediates GSC self-renewal and maintenance[59]. Silencing SOX2 induces ISG expression in GSCs, echoing our observation of induced ISG expression and reduced GSC growth upon KO of PUS7 in GSCs. Both our study and the recent study by Zhu et al support a negative correlation between ISG expression and GSC self-renewal and maintenance.

The clinical significance of this study is the discovery of chemical inhibitors of PUS7 in suppression of GBM tumorigenesis. With the rapid growth of our understanding on epitranscriptomes in physiology and disease, therapeutic strategies targeting the epitranscriptomic machineries are evolving. Although an association between pseudouridine modification and cancer has been made, inhibitors for pseudouridine synthases are lacking, preventing pseudouridine-targeting therapeutic development. In this study, we have used a structure-based virtual screening coupled with *in vitro* enzymatic activity screening for inhibitor discovery for PUS7. The identified inhibitors were able to reduce pseudouridine levels and inhibit GSC growth and tumorigenesis. These inhibitors could be exploited as potential therapeutic candidates for targeting PUS7 in GBM and other cancers. Moreover,

the screening strategies we used here may be applicable to other epitranscriptomic machineries for discovery of chemical therapeutics.

Methods

Cell culture

GSCs were derived from newly diagnosed grade IV GBM patients. GSCs and NSCs were maintained in spheres in DMEM-F12 medium supplemented with 2 mM L-glutamine, 27.4 mM HEPES, B27, 20 ng ml^{-1} EGF, 20 ng ml^{-1} FGF and 5 μg ml^{-1} heparin as described[20]. Established GBM cells were maintained in DMEM medium supplemented with 2 mM L-glutamine and 10% FBS. All cultures were mycoplasma-free as confirmed using MycoAlert PLUS Mycoplasma Detection Kit (Lonza). GSCs or NSCs were treated with PUS7 inhibitors at indicated concentration for 72 h. GSCs were treated with IFNα at indicated doses for 6 days. Details for materials including cell culture reagents were in Supplemental table 11.

Human Subjects Research

Specimens without identifiers from leftover surgical tissues were used in this study. The information was evaluated and determined to not involve human subjects research by City of Hope Institutional Review Board (IRB).

Animals

All animal-related work was performed under the IACUC protocol 05050 approved by the City of Hope Institutional Animal Care and Use Committee. Mice were housed in rooms with 20 to 24 °C room temperature, 30–70 % humidity, and a 12/12 hours light/dark cycle.

Plasmid DNA

shRNAs were cloned into the pHIV7-GFP lentiviral vector. sgRNAs were cloned into lentiCRISPR v2 vector (Addgene plasmid # 52961) or lentiCRISPR v2-Blast vector (Addgene plasmid # 83480). The sequences for shRNAs and sgRNAs were listed in Supplemental table 11. The WT or mutant PUS7 (D256A)[47] was cloned into the CSC lentiviral vector. The reporter plasmids were prepared by inserting 6 x CGG or 6 x CGA sequences before the firefly luciferase coding region in the pmirGlo luciferase expression vector (Promega) to obtain the 6 x Arg (CGG) or the 6 x Arg (CGA) reporter plasmid. The TYK2 fragment plasmids were cloned by replacing the eGFP sequences in the pLENTI-DDK-puro-eGFP vector (Addgene plasmid #123299) with the WT or mutant TYK2 fragment (aa 100- aa 264).

Viral preparation and transduction

Lentiviruses were prepared using 293T cells as described[60]. GSCs were transduced by incubating with lentivirus and 4 μg ml^{-1} polybrene (AmericanBio) for 24 h. The sgRNA-expressing lentivirus transduced cells were selected with 5 μg ml^{-1}blasticidin (Gibco) or 2 μg ml^{-1}puromycin (Gibco).

GBM database analysis

Data from the CGGA, the Rembrandt, the TCGA and the Gravendeel datasets were accessed through the GlioVis portal[61] (http://gliovis.bioinfo.cnio.es/). The detailed setting for patient survival and gene expression analyses was listed in Supplementary Table 1 and 2. Raw data for patient survival and gene expression analyses downloaded from the GlioVis portal were included in Supplementary Table 12. For PUS7 and ISG correlation analysis, IDH wild type GBM patient data from TCGA GBM HG-U133A dataset were used. The single-sample GSEA (ssGSEA) analysis was performed using the Gene Set Variation Analysis (GSVA) package 1.40.0[62].

Immunohistochemistry

Immunohistochemistry analysis was performed on GBM tissue microarray (US Biomax, GL806f) using antibodies for SOX2 and PUS7. The intensity of the PUS7 signal was quantified on a relative scale from 1 to 3 (1= low, 2=medium, and 3=high).

RT-PCR and Western blot

RT-PCR and Western blot were performed as described[26]. Primers for RT-PCR and antibodies for Western blot were listed in Supplemental table 11. Bio-Rad's Image Lab 6.0 was used for Western blot data analysis.

Cell growth, sphere formation and limiting dilution assays

GSC growth, sphere formation and limiting dilution assays were performed as described[20]. For growth, GSCs were seeded at 5×10^4 cells per well in 24-well plates and cultured for 7 days. Cell growth was monitored by cell counting using a hemocytometer. For sphere formation, GSCs were seeded at 1 cell per well in 96-well plates or 100 cells per well in 48-well plates and cultured for 2 weeks. Spheres were counted under microscope. For limiting dilution assay, GSCs were seeded into 96-well plates at 1, 5, 10, 20, 50 and 100 cells per well. The number of sphere-forming wells was recorded in two weeks. The limiting dilution analysis was performed using the extreme limiting dilution analysis software at http://bioinf.wehi.edu.au/software/elda.

Cell cycle analysis

The cell cycle analysis was performed using FxCycle™ PI/RNase Staining Solution. Propidium iodide staining of DNA content in fixed cells was analyzed by flow cytometry to determine the cell cycle status.

GSC transplantation and PUS7 inhibitor treatment

One week after viral transduction, 2×10^5 GSCs were transplanted into the frontal lobes of mouse brain (AP +0.6 mm, ML +1.6 mm and DV −2.6 mm) by stereotaxic intracranial injection For PUS7 inhibitor treatment, one week after GSC transplantation, tumors were detected by bioluminescence imaging and mice were treated with 5 μl of 400 nM PUS7 inhibitor C17 in PBS per mouse, corresponding to a dose of 25.9 ng/Kg C17 for a 25 g mouse for PBT003 cells, or 5 μl of 1 μM C17 in PBS per mouse, corresponding to a dose of 64.9 ng/Kg C17 for a 25 g mouse for PBT707 cells, or vehicle control, by intratumoral

injection once a week for four weeks using the same coordinates for GSC transplantation. Tumor growth was monitored by bioluminescence imaging every other week for six to nine weeks. The bioluminescence intensity was quantified using Spectral Instruments Imaging-AMIView 1.7.061. Mice were euthanized when one or more of the early euthanasia criteria (failure to eat food/ drink water for 24 h; failure to make normal postural adjustments/ display normal behavior; obvious distress such as posture hunched, unresponsive; weight loss > 20%) were met. The survival of mice was recorded.

Virtual screen for PUS7 inhibitor

The virtual screen was performed using in-house developed LiVS (Ligand Virtual Screening Pipeline) as described[63]. The PUS7 catalytic center was used as a pocket for the virtual screening. A small molecule compound library containing the NCI-DTP (developmental therapeutics program) compounds and the FDA-approved drugs was used to identify inhibitor hits for PUS7. The available compounds from the top 100 hits were validated.

In vitro PUS7 activity assay

For PUS7 activity assay, 100 μM candidate compound was added to 1 μg PUS7 recombinant protein, 0.5 μg in vitro T7 transcribed tRNA-Glu substrates, 20 U rRNasin, 100 mM Tris-HCl pH 8.0, 100 mM Ammonium acetate, 2 mM DTT, 0.1 mM EDTA, and 5 mM $MgCl_2$, in 25 μl reaction, and incubated at 37 °C for 1 h. RNA was purified by ethanol precipitation and subjected to MS analysis to quantify pseudouridine level. The small molecule screening information is summarized in Supplemental Table 13.

MS analysis for pseudouridine levels

Quantification of pseudouridine level in RNA samples was performed as described[11] with modifications. Briefly, 200 ng RNA samples were digested with 1 U nuclease P1 at 42 °C for 1–6 hours. Then 2.5 μl MES buffer (pH 6.5), 0.25 μl rSAP (1,000 U/ml), and 2.25 μl nuclease-free water were added, and incubated at 37 °C overnight. Ψ/U levels were analyzed using LC-MS/MS (Agilent 6490 QQQ or AB SCIEX QTRAP 5500).

Small RNA DM-Ψ-seq

Small RNA was extracted using MEGAclear Transcription Clean-Up Kit (Invitrogen). For library preparation, small RNA fraction was demethylated by AlkB protein, recovered by phenol chloroform extraction, labeled by CMC and then treated with Na_2CO_3. RNA was labeled with CMC as described[11,14] with modifications. Briefly, 10 μg RNAs were fragmented into 150–200 nt fragments. RNA was recovered by ethanol precipitated and denatured at 80 °C for 5 min. 5 μg denatured RNA was added to 100 μl BEU buffer with or without 0.2M CMC. The CMC reaction was carried out at 37 °C for 20 min, followed by ethanol precipitation. Recovered RNA was re-dissolved in 50 μl Na_2CO_3 buffer, incubated at 37 °C for 6 h, followed by ethanol precipitation. Library preparation was performed according to the eCLIP protocol as described[64] with modifications. RNA samples were dephosphorylated with CIP. 3’ adaptor ligation was performed with RNA T4 ligase 2 truncated KQ, followed by 5’ deadenylase and RecJf treatment. Reverse transcription was performed with Superscript III reverse transcriptase, and cDNA was treated with 1 μl RNase

H. 5' linker ligation was performed with T4 RNA ligase 1 high concentration. cDNA was amplified by PCR. The PCR products were purified and sequenced on Illumina Hiseq 2000 or X10.

Primer extension and Northern blot

Primer extension and Northern blot were performed as described[14,65]. For primer extension, CMC-labeled small RNA fractions were mixed with biotin-labelled RT primer, followed by reverse transcription. RT products were separated on Urea-PAGE, transferred to Nylon membrane, and detected by chemiluminescent nucleic acid detection module (Thermo). For Northern blot, RNA samples were separated on Urea-PAGE, transferred to Nylon membrane, and hybridized with DIG-labeled probe. The membrane was washed and blocked using DIG Wash and Block Buffer Set (Roche).

Expression analysis of tRNA-derived fragments (tRFs)

The reads number of tRFs was calculated from the FASTQ files and combined with the aligned information from the aligned file to determine the abundance and location of tRFs. Only tRFs with reads number >100 was used for analysis. Differential expression analysis of tRFs in control and PUS7 KO GSCs (three biological replicates per condition) was performed using the DESeq2 R package (version 1.16.1). tRFs with an adjusted p value < 0.01 and fold change (KO/WT) > 2 were assigned as differentially expressed.

Transcriptome-wide Ψ sequencing

CMC is used for transcriptome-wide Ψ profiling as described[10,11]. 500 ng poly A+ RNA samples were fragmented, labeled by CMC, and then treated with Na_2CO_3. Library preparation was similar to that described in small RNA DM-Ψ-seq. Ψ sequencing of rRNA was performed similarly.

Identification of Ψ sites on tRNA, rRNA, and mRNA

For small RNA DM-Ψ-seq data, transcriptome-wide or rRNA Ψ seq data, a random barcode of 10 nt was added to the 5' end of Reads 2 to remove PCR duplication, so only Reads 2 in raw sequencing data were used for further analysis. The adapter sequences were trimmed by Cutadapt (Version 2.10). The minimum quality threshold was set to 20, and the minimum length required for reads after trimming was 30 nt. The remaining reads were further processed by removing the first 10 nt random barcode in the 5′ end, and then mapped with Bowtie aligner (Version 1.2.2), with parameters set as "*bowtie -a --best --strata --chunkmbs 2000*".

For identification of Ψ in small RNA, we considered position i to be a Ψ site with the following criteria: (1) CMC coverage > 50; (2) stop Reads number > 5 in CMC sample; (3) stop rate (SR) < 1% in BEU sample; (4) SR (CMC-BEU) difference > 4%; (5) SR fold change (CMC/BEU) > 4; (6) the adjusted p value of matched sample < 0.05; (7) the Ψ site appears in all three independent replicates. For identification of PUS7-dependent Ψ in small RNA dataset, we consider position i to be a PUS7-dependent Ψ site with the following criteria: (1) Position i was considered a Ψ site in WT GSCs; (2) SR (WT_{CMC} −

PUS7KO$_{CMC}$) difference > 4%; (3) SR fold change (WT$_{CMC}$ / PUS7KO$_{CMC}$) > 1.5; and (4) adjusted p value < 0.05. In some cases, conditions 2 and 3 were not met at the same time.

For identification of Ψ in rRNAs, we considered position i to be a Ψ site with the following criteria: (1) coverage (CMC) > 200; (2) CMC stop rate > 5%; (3) SR Fold Change (CMC/BEU) > 2; (4) SR difference (CMC-BEU) > 3%; (5) adjusted p value < 0.05; and (6) the Ψ site must appear in at least two replicates.

For identification of Ψ on mRNAs, we considered position i to be a Ψ site with the following criteria: (1) CMC coverage > 50; (2) CMC stop rate > 6%; (3) SR (CMC-BEU) difference > 5; (4) SR Fold Change (CMC/BEU) > 5; (5) adjusted p value < 0.05; and (6) the Ψ site appears in at least two replicates. For identification of PUS7-dependent Ψ sites, we consider position i to be true with the following criteria: (1) position i was considered a Ψ site in WT GSCs; (2) the difference of SR between the WT-CMC (+) samples and the matched PUS7KO-CMC (+) samples must be at least 5%.

Motif discovery and GO enrichment analysis

For analysis of sequence consensus, a 10-nt sequence next to each Ψ site was retrieved. These sequences were subjected to DREME algorithm in MEME suite (Version 5.1.1) for discovery of enriched motives[66]. The shuffled input sequences were used as the background to eliminate potential false positive caused by nucleotide composition. GO enrichment analyses were performed using a cluster Profiler (version 3.14.3)[67].

TMT-based quantitative proteomics analysis

Proteins were reduced and alkylated with TCEP and iodoacetamide and precipitated in 10% trichloroacetic acid, then digested overnight with Trypsin/ LysC (protein : protease ratio = 80:1). Resulting peptides were purified and labeled with TMT reagents. High pH reverse phase chromatography was performed using a Thermo Ultimate 3000 HPLC system (Thermo) with a 250 mm Zorbax extend C18 column (Agilent, ID 4.6 mm, particle size 5 μm) and one hour gradient from 97% ammonium bicarbonate, pH 8, 3% to 40% acetonitrile. 96 fractions were collected and combined into 24 fractions. These fractions were analyzed on an Orbitrap Fusion Lumos mass spectrometer with a 5 mm C18 PepMap 100 μ-precolumn (ID 300 μm), a 75 μm by 50 cm PepMap RSLC C18 analytical column (Thermo), and an Easy-Spray ion source (Thermo Scientific). Peptides were eluted. MS3 quant spectra were acquired in the Orbitrap, while MS2 fragment spectra were acquired in the linear trap.

RNA-seq

Total RNAs isolated from control or PUS7 KO PBT003 GSCs were subjected to RNA-seq. Library construction of 300 ng total RNA from each sample was made using KAPA mRNA HyperPrep Kit (Illumina Platforms). Libraries were purified using AxyPrep Mag PCR Clean-up kit. Sequencing was performed on an Illumina® Hiseq 2500 (Illumina) instrument using the TruSeq SR Cluster Kit V4-cBot-HS to generate 51 bp single-end reads. The raw counts of each gene were generated by running HTSeq (v0.6.1p1) against GRCh37 GTF file (Ensembl release 87). RPKM (Reads Per Kilobase of transcript, per Million mapped reads)

was calculated using the count data and gene length. Gene set enrichment analysis[68,69] was performed for differentially expressed genes from RNA-seq using the GSEA 4.1.0 software and the MSigDB version v7.2.

OP-puro incorporation analysis

The Op-puro incorporation assay was performed using the Click-iT Plus OPP Alexa Fluor™ 647 Protein Synthesis Assay Kit. Data were analyzed by Flowjo 10.7.1.

Nascent protein synthesis analysis

Nascent protein synthesis was performed as described[65] with modifications. Cells in log phase were pre-treated with methionine-free DMEM medium, followed by L-azidohomoalanine (AHA) labeling. Total proteins were quantified, and then labeled with Cy3. The Cy3-labeled proteins were separated using gradient SDS-PAGE. Protein gels were stained with silver stain kit.

Codon bias analysis

The global frequency of a specific codon was obtained by calculating the codon frequency of each gene annotated by Refseq, and the codon frequency of the TYK2 was calculated. The ranking of the codon frequency of the TYK2 among that of the global transcriptome was indicated. The other codons encoding the same amino acid were used as controls.

Luciferase Reporter Assay

Control or PUS7 KO GSCs were transfected with luciferase reporter plasmids using Lipofectamine 3000. After 48 h, cells were assayed by Dual-Luciferase Reporter Assay System. The renilla luciferase was used as a normalization control.

Polysome profiling analysis

We followed the procedure reported previously for polysome fractionation[70] with the following modifications. (1) GSCs were treated with 100 μg/ml CHX for 7 min, flash frozen in liquid N2 and stored at −80 degree. (2) The lysis buffer contains 100 μg/ml CHX. Total RNAs were isolated by using the Direct-zol RNA Microprep with on-column DNase-I digestion. RT-PCR was performed to determine TYK2 expression in each fractionation.

Statistics and reproducibility

Unpaired Student’s t-test was used for statistical analysis between two groups, One-way ANOVA test was used for statistical analysis of more than two groups using GraphPad Prism 8 software with default setting. The method of statistical analysis was indicated in each figure legend. Values were presented as *$p<0.05$, **$p<0.01$, ***$p<0.001$ with exact p values shown in the legend of each figure. Error bars are s.e. of the mean unless stated otherwise. Log-rank test was used for animal survival analysis. Experiments were performed with sample size n greater than or equal to 3 replicates and results from representative experiments were confirmed in at least two independent experiment repeats and multiple cell lines. For animal study, 6–12-week-old male and female NSG mice (from the Jackson Laboratory) were used in age- and gender-matched manner. A sample size determination

(n greater than or equal to 5 mice) was calculated using t-test for two-group independent samples to reach power of 0.8 and the significance level of 0.05 based on our preliminary study. $p < 0.05$ was considered statistically significant. When monitoring tumor growth, investigators were blinded to the group allocation during bioluminescence imaging and aware of group allocation when assessing the outcome. For other experiments, sample size was determined empirically based on our preliminary or previous studies, experiments were not randomized, and the Investigators were not blinded to allocation during experiments and outcome assessment. No data were excluded from analyses. Further information on research design is available in the Nature Research Reporting Summary linked to this article.

Data availability

Data that support the findings of this study have been deposited in the Gene Expression Omnibus (GEO) under accession code GSE147382 for RNA-seq data and GSE147342 for pseudouridine-seq data. Human data were derived from the CGGA, the Rembrandt, the TCGA and the Gravendeel datasets. Data derived from these resources is available in the GlioVis portal (http://gliovis.bioinfo.cnio.es/). tRNA sequences from GtRNAdb and human genome sequences from GCF_000001405.25_GRCh37.p13 were used for this study. Source data for Figures 1 to 8 and Extended Data Figures 1 to 8 have been provided as Source Data files. Supplementary Tables 1 to 13 are provided. All other data supporting the findings of this study are available from the corresponding authors upon reasonable request.

Extended Data

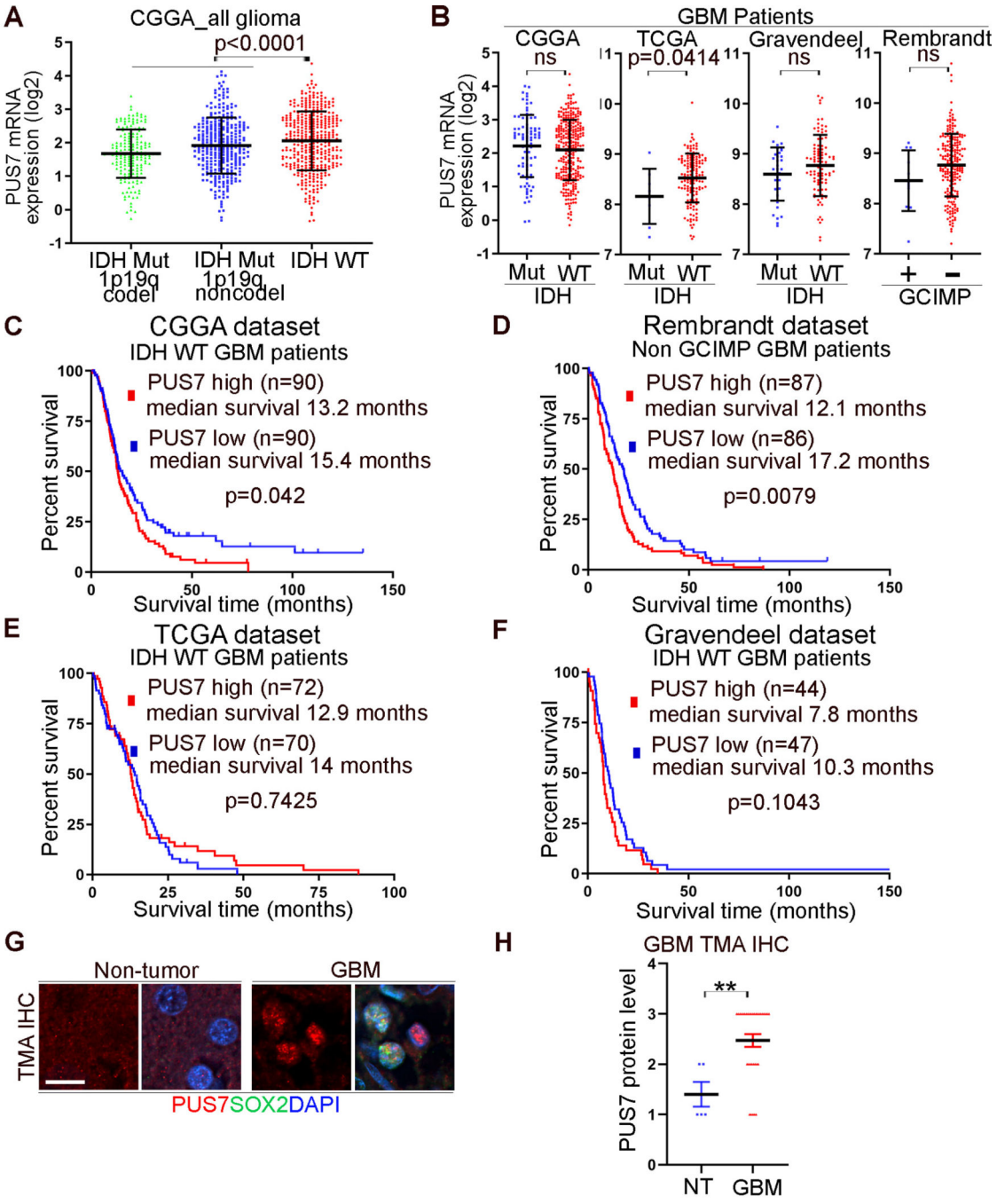

Extended Data Fig. 1. High level of PUS7 expression correlates with poor prognosis in GBM patients

(A) The expression of PUS7 in all glioma patients stratified by the IDH mutation status and 1p19q chromosome co-deletion status from the CGGA dataset (n=182 IDH mut 1p19q codel patients, n=315 IDH mut 1p19q noncodel patients, n=392 IDH WT patients). **(B)** The expressions of PUS7 in GBM patients stratified by IDH mutation status or GCIMP status from the CGGA (n=90 Mut patients and n=288 WT patients), TCGA (n=8 Mut

patients and n=142 WT patients), Gravendeel (n=33 Mut patients and n=95 WT patients), and Rembrandt (n=11 GCIMP patients and n=208 Non-GCIMP patients) datasets. **(C-F)** Kaplan-Meier survival curves with log-rank analysis to assess the correlation between PUS7 expression and overall survival of IDH WT GBM patients in the CGGA dataset (**C**), TCGA dataset (**E**), and Gravendeel dataset (**F**) or non GCIMP GBM patients in the REMBRANDT dataset (**D**). (**G**) The expression of SOX2 and PUS7 in GBM patients and in non-tumor control samples in GBM tissue microarray analyzed by immunohistochemistry (IHC). Scale bar: 10 μm. (**H**) Quantification of the expression level of PUS7 in GBM patients and in non-tumor control samples analyzed by IHC. n = 34 individuals for GBM patients and 5 individuals for non-tumor control group. Error bars represent SD of the mean for panels **A** and **B**. Error bars represent SE of the mean for panel **H**. Two-tailed Student's t test for panels **A** and **B** (ns: not statistically significant. p=0.2844 for CGGA, p=0.1533 for Gravendeel, and p=0.1095 for Rembrandt). **p<0.01 (p=0.002) by one-tailed Student's t-test for panel **H**.

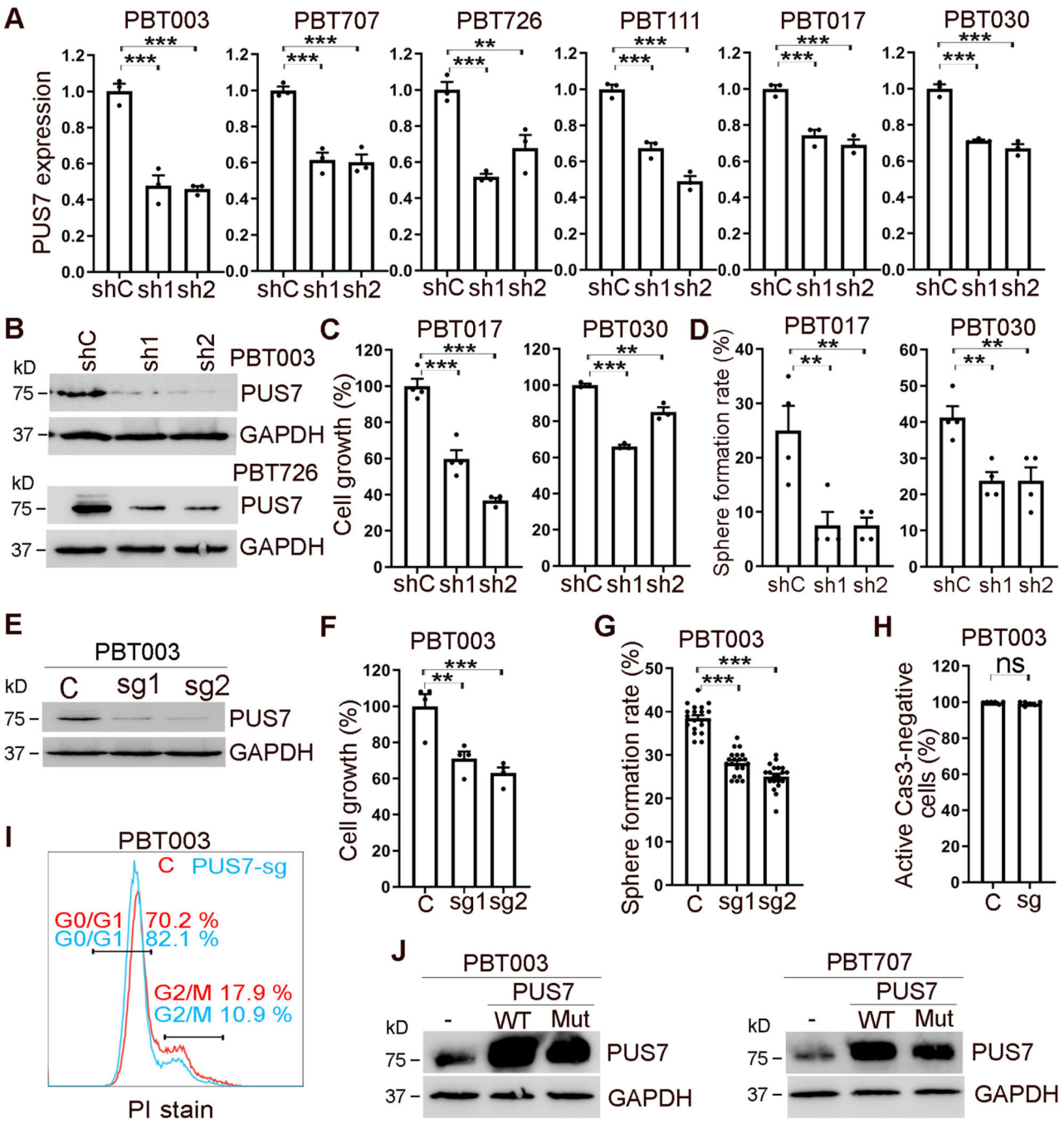

Extended Data Fig. 2. PUS7 regulates GSC growth and self-renewal

(A) RT-PCR analysis of PUS7 knock down (KD) in GSCs (PBT003, PBT707, PBT726, PBT111, PBT017, and PBT030) transduced with lentivirus expressing control shRNA (shC) or PUS7 shRNA (sh1 and sh2). n=3 technical replicates. p=0.0002 for sh1 and p=0.0002 for sh2 in PBT003; p=0.0005 for sh1 and p=0.0004 for sh2 in PBT707; p=0.0008 for sh1 and p=0.0066 for sh2 in PBT726; p=0.0003 for sh1 and p<0.0001 for sh2 in PBT111; p=0.0009 for sh1 and p=0.0004 for sh2 in PBT017; p<0.0001 for sh1 and p<0.0001 for sh2 in PBT030. **(B)** Western blot analysis of PUS7 KD in GSCs (PBT003 and PBT726).

The uncropped blot images for the cropped images shown here are in the source data. Repeated twice with similar results. **(C)** Cell growth of GSCs (PBT017 and PBT030) transduced with lentivirus expressing control shRNA (shC) or PUS7 shRNA (sh1 and sh2). n=4 cell culture replicates. p<0.0001 for sh1 and p<0.0001 for sh2 in PBT017; p<0.0001 for sh1 and p=0.0013 for sh2 in PBT030. **(D)** Sphere formation of GSCs (PBT017 and PBT030) transduced with lentivirus expressing shC or PUS7 shRNA (sh1 and sh2). n=4 cell culture replicates. p=0.006 for sh1 and p=0.006 for sh2 in PBT017; p=0.0063 for sh1 and p=0.0063 for sh2 in PBT030. **(E)** Western blot analysis of PUS7 in PBT003 GSCs transduced with lentivirus expressing control sgRNA or sgRNA for PUS7 (sg1 and sg2). The uncropped blot images for the cropped images shown here are in the source data. Repeated four times with similar results. **(F)** Cell growth of PBT003 GSCs transduced with lentivirus expressing control sgRNA or sgRNA for PUS7. n=4 cell culture replicates. p=0.0043 for sg1 and p=0.0009 for sg2. **(G)** Sphere formation of PBT003 GSCs transduced with lentivirus expressing control sgRNA or sgRNA for PUS7. n=20 sphere-forming culture replicates. **(H)** Active Caspase 3 (Cas3) analysis of PBT003 GSCs transduced with lentivirus expressing control sgRNA or sgRNA for PUS7. p<0.0001 for sg1 and p<0.0001 for sg2. n=5 cell culture replicates. **(I)** Cell cycle analysis of PBT003 GSCs transduced with lentivirus expressing control sgRNA or sgRNA for PUS7. **(J)** Western blot analysis showing overexpression of the WT and the mutant PUS7 in PBT003 and PBT707 GSCs. The uncropped blot images for the cropped images shown here are in the source data. Repeated three times with similar results. Error bars are SE of the mean for this figure. **p<0.01 and ***p<0.001 by One-way ANOVA and Dunnett's multiple comparisons test for panels **A**, **C**, **D**, **F**, and **G**. ns: not statistically significant (p=0.1372) by one-tailed Student's t-test for panel **H**.

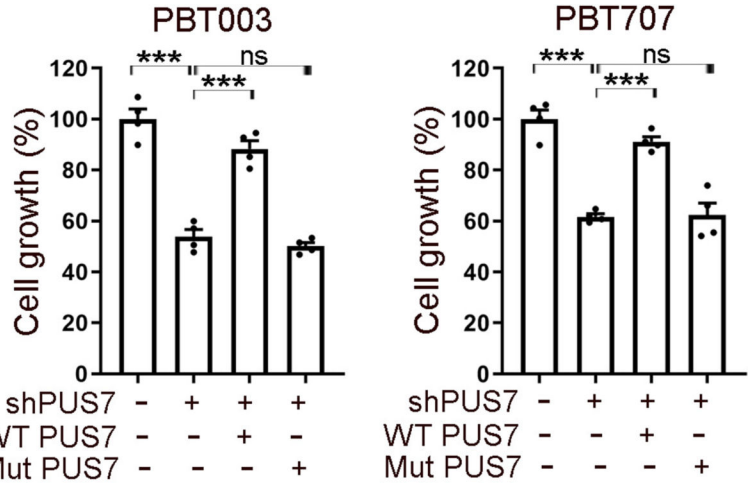

Extended Data Fig. 3. PUS7 regulates GSC growth in a catalytic activity dependent manner

The WT but not the mutant (Mut) PUS7 rescued PUS KD-induced growth inhibition in PBT003 and PBT707 GSCs. n=4 cell culture replicates. p<0.0001 for shPUS7 (−) and PUS7 (−) vs shPUS7 (+) and PUS7 (−), p<0.0001 for shPUS7 (+) and PUS7 (−) vs shPUS7 (+) and WT PUS7 (+), ns: p=0.7179 for shPUS7 (+) and PUS7 (−) vs shPUS7 (+) and Mut PUS7 (+) in PBT003; p<0.0001 for shPUS7 (−) and PUS7(−) vs shPUS7 (+) and PUS7(−),

p<0.0001 for shPUS7 (+) and PUS7 (−) vs shPUS7 (+) and WT PUS7 (+), ns: p=0.9976 for shPUS7 (+) and PUS7 (−) vs shPUS7 (+) and Mut PUS7 (+) in PBT707. Error bars are SE of the mean for this figure. ***p<0.001 and ns: not statistically significant (p>0.05, defined above) by One-way ANOVA and Dunnett's multiple comparisons test for this figure.

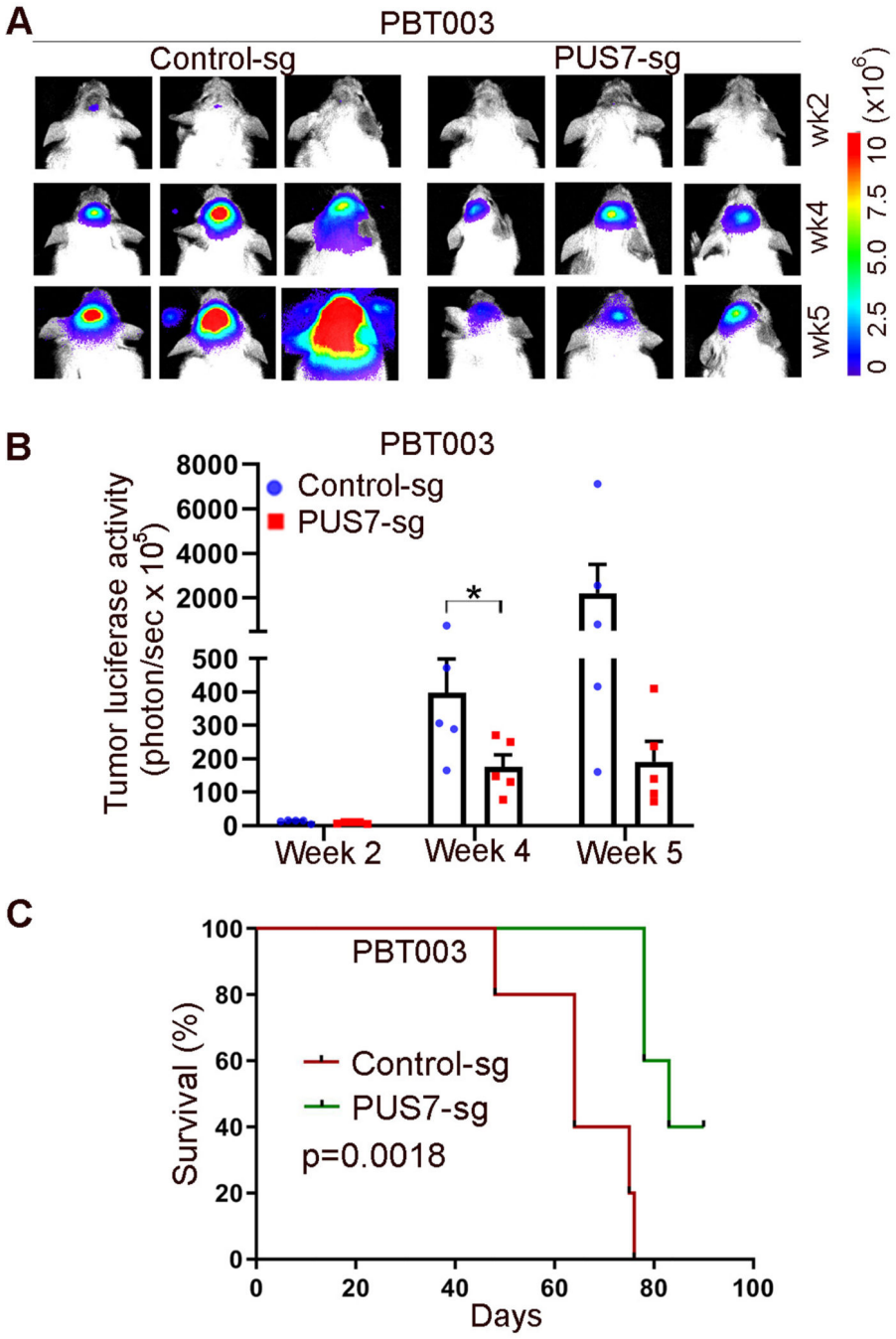

Extended Data Fig. 4. Inhibition of PUS7 suppresses tumor progression

(A) Bioluminescent images of brain tumors in NSG mice transplanted with PBT003 GSCs that were transduced with control sgRNA (Control-sg) or PUS7 sgRNA (PUS7-

sg). **(B)** Quantification of the bioluminescence intensity of tumors after PBT003 GSC transplantation. n=5 mice for each group. Error bars represent SE of the mean. *p<0.05 (p=0.037) by one-tailed Student's t-test. **(C)** The survival curves of NSG mice transplanted with PBT003 GSCs transduced with control sgRNA or PUS7 sgRNA. n=5 mice for each group. The X axis represents days after GSC transplantation. Log-rank test for mice survival.

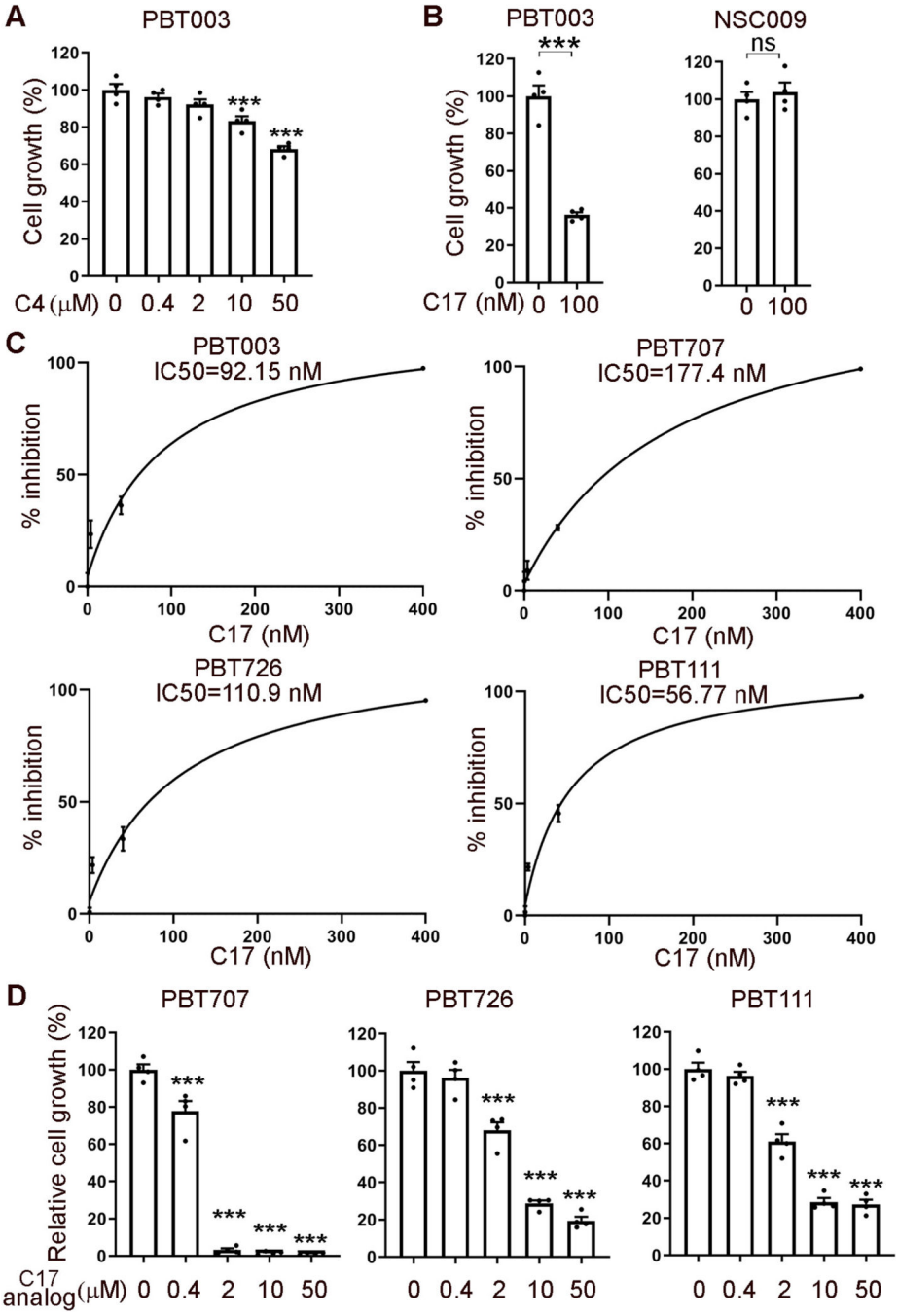

Extended Data Fig. 5. PUS7 inhibitors suppress GSC growth

(A) Cell growth of PBT003 GSCs treated with the C4 PUS7 inhibitor. n=4 cell culture replicates. p=0.0009 for 10 μM and p<0.0001 for 50 μM condition. **(B)** Cell growth of PBT003 GSCs or NSC009 NSCs treated with the C17 PUS7 inhibitor. n=4 cell culture replicates. p<0.0001 for PBT003 and ns: p=0.2831 for NSC009. **(C)** IC50 test for C17 compound in GSCs (PBT003, PBT707, PBT726, and PBT111). For each GSC, n=4 cell culture replicates for each treatment condition. **(D)** Cell growth of GSC (PBT707, PBT726, and PBT111) treated with the C17 analog compound. n=4 cell culture replicates. p=0.0002, <0.0001, <0.0001, <0.0001 for 0.4, 2, 10, 50 μM conditions respectively in PBT707; p<0.0001 for 2, 10, 50 μM conditions in PBT726; p<0.0001 for 2, 10, 50 μM conditions in PBT111. Error bars are SE of the mean. ***p<0.001 by One-way ANOVA and Dunnett's multiple comparisons test for panels **A** and **D**. ***p<0.001 and ns: not statistically significant (p>0.05, defined above) by one-tailed Student's test for panel **B**.

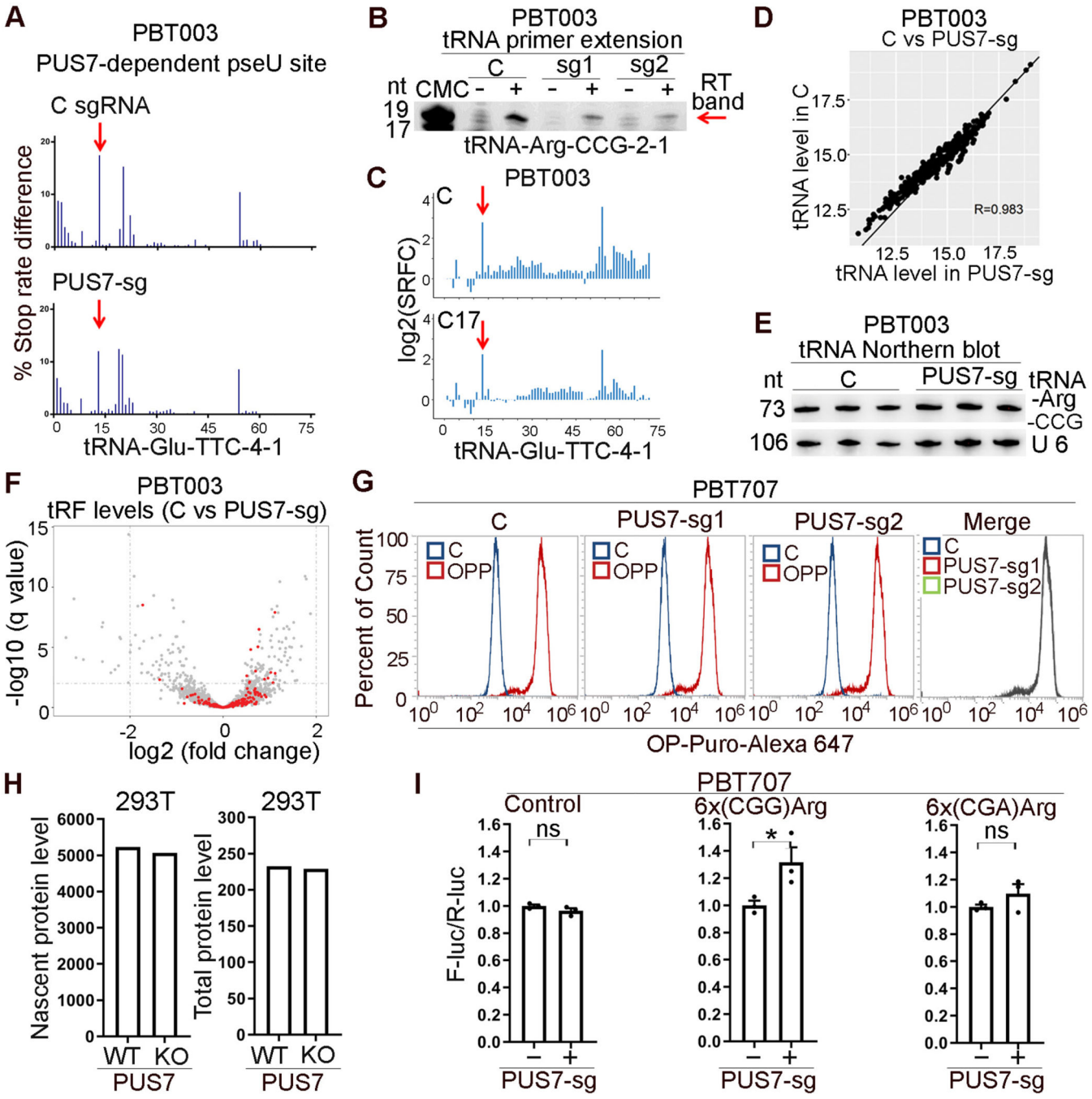

Extended Data Fig. 6. The pseudouridine modification profile in GSCs

(A) A representative PUS7-dependent pseudouridine site identified by small RNA DM-Ψ-seq in PBT003 GSCs. **(B)** Validation of the PUS7-dependent pseudouridine site in tRNA-Arg-CCG-2–1 in PUS7 KO PBT003 GSCs by primer extension assay. The uncropped blot images for the cropped images shown here are in the source data. Repeated twice with similar results. **(C)** A representative PUS7-dependent pseudouridine site in tRNA-Glu-TTC-4–1 in control or C17-treated PBT003 GSCs. **(D)** Pearson correlation analysis for global tRNA abundance in control and PUS7 KO PBT003 GSCs. (**E**) Expression of tRNA-

Arg-CCG in control and PUS7 KO PBT003 GSCs examined by Northern blot analysis. U6 was used as a loading control. The uncropped blot images for the cropped images shown here are in the source data. Repeated twice with similar results. (**F**) Analysis of tRF abundance in control and PUS7 KO PBT003 GSCs. Red dots: tRFs derived from tRNAs with PUS7-dependent pseudouridine sites. The q value was calculated by Cochran Mantel Haenszel test and adjusted by BH methods. **(G)** The OP-puro incorporation analysis of control and PUS7 KO PBT707 GSCs. **(H)** Nascent protein synthesis and total protein level analysis of control and PUS7 KO 293T cells. **(I) A** luciferase reporter assay to test tRNA translation efficiency in control and PUS7 KO PBT707 cells. n=3 cell culture replicates. Error bars are SE of the mean. *p<0.05 (p=0.0251), and ns: not statistically significant [p>0.05, p=0.0921 for control, p=0.0251 for 6x(CGG)Arg, and p=0.1238 for 6x(CGA)Arg] by one-tailed Student's t-test.

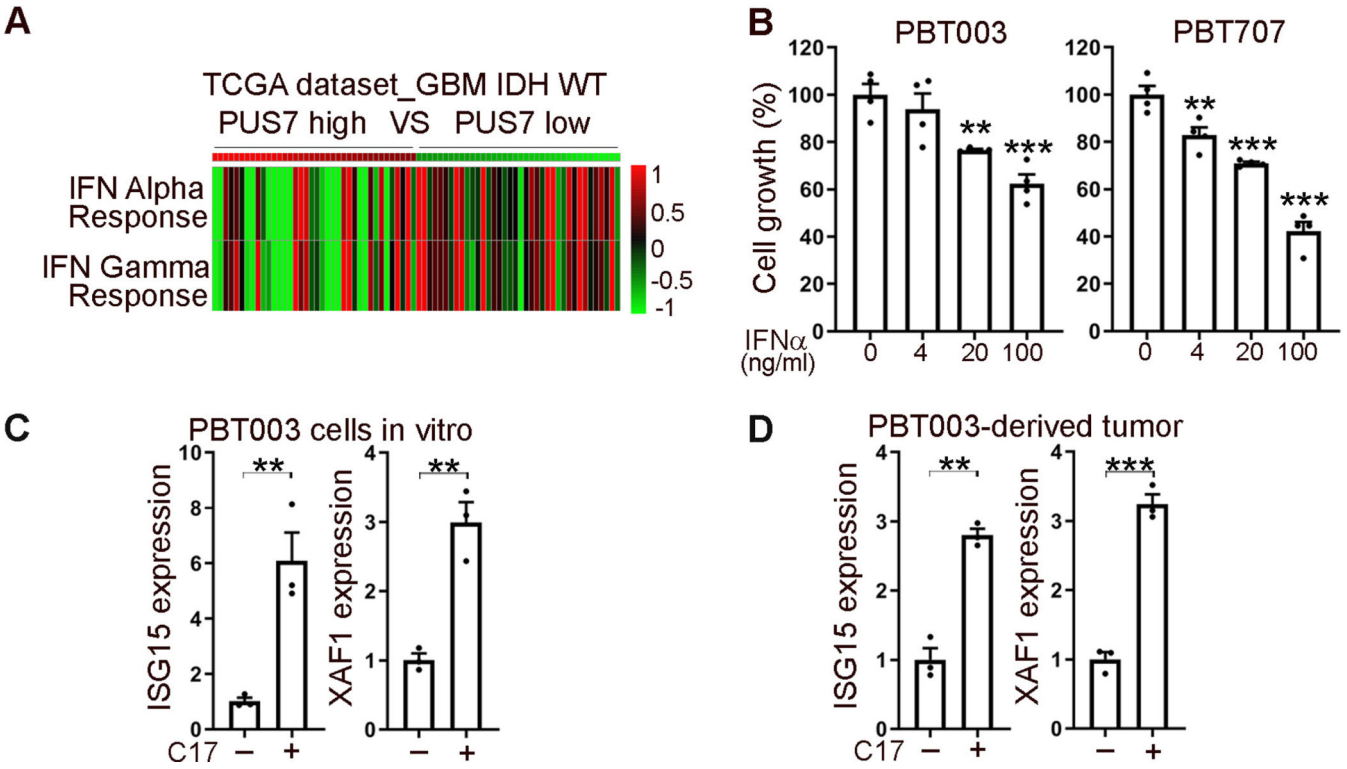

Extended Data Fig. 7. PUS7 regulates IFN pathway in GSC

(A) Correlation analysis of PUS7 expression and IFN gene signature (IFN alpha response gene signature and IFN gamma response gene signature) analyzed by ssGSEA in GBM patients from the TCGA dataset. **(B)** The growth of PBT003 and PBT707 GSCs treated with IFNα. n=4 cell culture replicates. p=0.0093 for 20 ng/ml and p=0.0002 for 100 ng/ml in PBT003; p=0.0064, <0.0001, <0.0001 for 4, 20, 100 ng/ml conditions, respectively, in PBT707. **(C)** RT-PCR of ISGs in C17 compound-treated PBT003 GSCs. n=3 technical replicates. p=0.0041 for ISG15 and p=0.0015 for XAF1. **(D)** RT-PCR of ISGs in C17 compound-treated tumor derived from PBT003 GSCs. n=3 technical replicates. p=0.0004 for ISG15 and p=0.0001 for XAF1. Error bars are SE of the mean. **p<0.01 and

***p<0.001 by One-way ANOVA and Dunnett's multiple comparisons test for panels **B**, and by one-tailed Student's t-test for panels **C** and **D**.

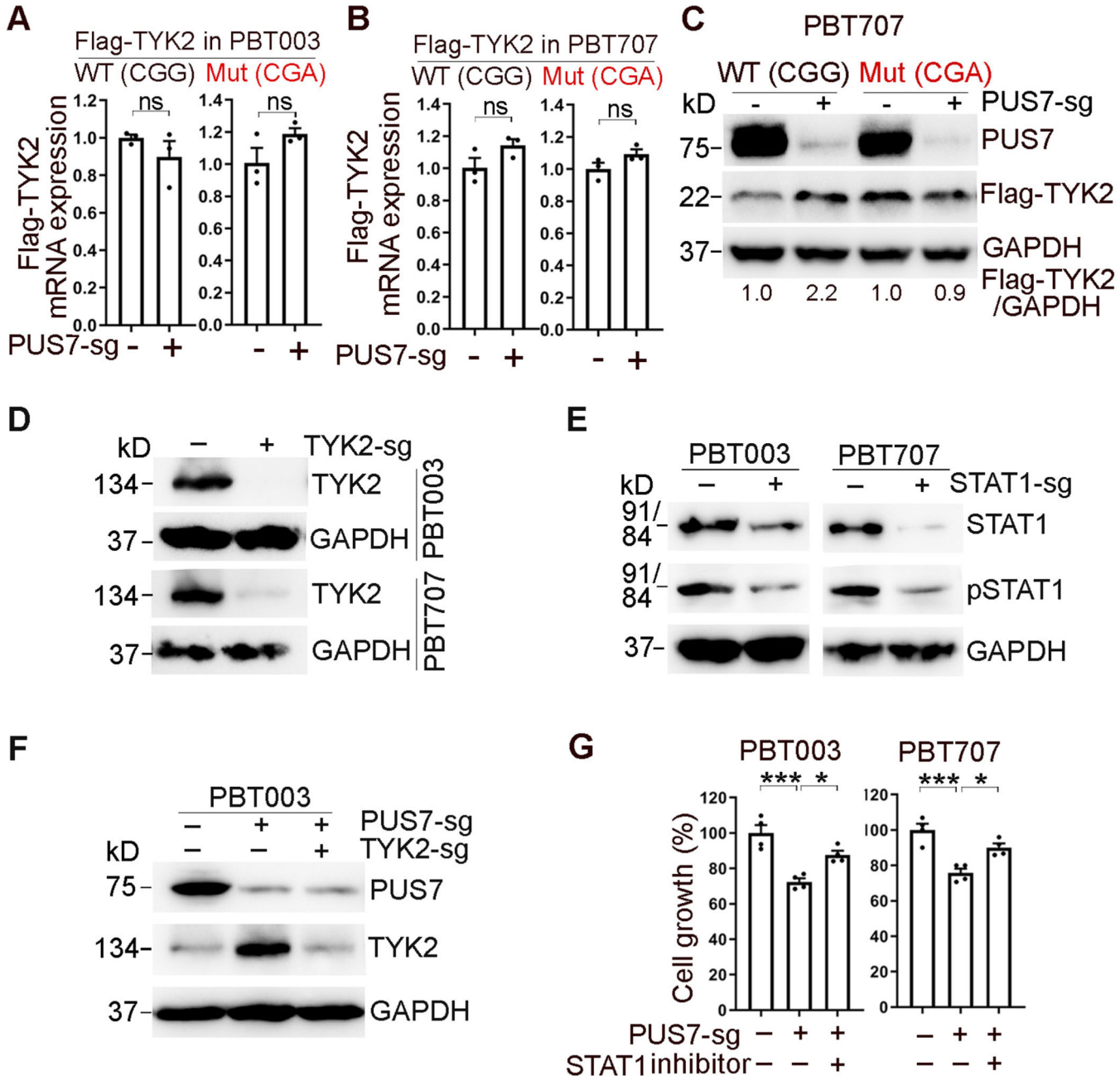

Extended Data Fig. 8. PUS7 regulates GSC growth through controlling TYK2-mediated IFN pathway

(A) RT-PCR analysis of WT or mutant TYK2 in PUS7 KO PBT003 GSCs. n=3 technical replicates. p=0.1533 for WT and p=0.0719 for Mut. **(B)** RT-PCR analysis of WT or mutant TYK2 in PUS7 KO PBT707 GSCs. n=3 technical replicates. p=0.0617 for WT and p=0.0625 for Mut. **(C)** Western blot analysis of WT or mutant TYK2 in PUS7 KO PBT707 GSCs. The uncropped blot images for the cropped images shown here are in the source

data. Repeated twice with similar results. **(D)** Western blot analysis of TYK2 in TYK2 KO PBT003 and PBT707 GSCs. The uncropped blot images for the cropped images shown here are in the source data. Repeated twice with similar results. **(E)** Western blot analysis of STAT1 and phosphorylated STAT1 (pSTAT1) in STAT1 KO PBT003 and PBT707 GSCs. The uncropped blot images for the cropped images shown here are in the source data. Repeated twice with similar results. **(F)** Western blot of PUS7 and TYK2 in PBT003 GSCs transduced with lentivirus expressing PUS7 sgRNA and/or lentivirus expressing sgRNA for TYK2. The uncropped blot images for the cropped images shown here are in the source data. Repeated twice with similar results. **(G)** The growth of PBT003 and PBT707 GSCs treated by the STAT1 inhibitor fludarabine with or without lentivirus expressing PUS7 sgRNA. n=4 cell culture replicates. p=0.0003 for PUS7sg (−) and STAT1 inhibitor (−) vs PUS7sg (+) and STAT1 inhibitor (−), p=0.0144 for PUS7sg (+) and STAT1 inhibitor (+) vs PUS7sg (+) and STAT1 inhibitor (−) in PBT003; p=0.0004 for PUS7sg (−) and STAT1 inhibitor (−) vs PUS7sg (+) and STAT1 inhibitor (−), p=0.0114 for PUS7sg (+) and STAT1 inhibitor (+) vs PUS7sg (+) and STAT1 inhibitor (−) in PBT707. Error bars are SE of the mean. *p<0.05, ***p<0.001, and ns: not statistically significant (p>0.05) by One-way ANOVA and Dunnett's multiple comparisons test for panels **G**, and by one-tailed Student's t-test for panels **A** and **B**.

Supplementary Material

Refer to Web version on PubMed Central for supplementary material.

Acknowledgements

The authors would like to thank Louise and Herbert Horvitz for their generosity and forethought, Yu Hsuan Lin and Xinqiang Li for their technical assistance, Xushen Xiong for his bioinformatics analysis suggestions. This work was supported by the Louise and Herbert Horvitz Charitable Foundation, the Sidell Kagan Foundation, California Institute for Regenerative Medicine TRAN1–08525, the National Institute of Aging of the National Institutes of Health R01 AG056305, RF1 AG061794, and R56 AG061171 to Y.S., the National Key R&D Program (nos. 2019YFA0110900 and 2019YFA0802200, the National Natural Science Foundation of China (nos. 21825701 and 91940304) to C.Y. and the National Center for Protein Sciences at Peking University. Research reported in this publication includes work performed in the Small Animal Imaging, Synthetic and Biopolymer Chemistry, Integrative Functional Genomics, and Analytical Cytometry Cores, was also supported by the National Cancer Institute of the National Institutes of Health under award number P30CA33572. The content is solely the responsibility of the authors and does not necessarily represent the official views of the National Institutes of Health. Part of the analysis was performed on the High-Performance Computing Platform of the Center for Life Science (Peking University). The results of TCGA database analysis published here are in whole or part based upon data generated by the TCGA Research Network: https://www.cancer.gov/tcga.

References

1. Machnicka MA, et al. MODOMICS: a database of RNA modification pathways−−2013 update. Nucleic acids research 41, D262–267 (2013). [PubMed: 23118484]
2. Nachtergaele S. & He C. Chemical Modifications in the Life of an mRNA Transcript. Annu Rev Genet 52, 349–372 (2018). [PubMed: 30230927]
3. Wu G, Yu AT, Kantartzis A. & Yu YT Functions and mechanisms of spliceosomal small nuclear RNA pseudouridylation. Wiley Interdiscip Rev RNA 2, 571–581 (2011). [PubMed: 21957045]
4. Charette M. & Gray MW Pseudouridine in RNA: what, where, how, and why. IUBMB life 49, 341–351 (2000). [PubMed: 10902565]
5. Davis FF & Allen FW Ribonucleic acids from yeast which contain a fifth nucleotide. The Journal of biological chemistry 227, 907–915 (1957). [PubMed: 13463012]

6. Karijolich J, Yi C. & Yu YT Transcriptome-wide dynamics of RNA pseudouridylation. Nature reviews. Molecular cell biology 16, 581–585 (2015). [PubMed: 26285676]
7. Hamma T. & Ferre-D'Amare AR Pseudouridine synthases. Chem Biol 13, 1125–1135 (2006). [PubMed: 17113994]
8. Spenkuch F, Motorin Y. & Helm M. Pseudouridine: still mysterious, but never a fake (uridine)! RNA biology 11, 1540–1554 (2014). [PubMed: 25616362]
9. Rintala-Dempsey AC & Kothe U. Eukaryotic stand-alone pseudouridine synthases - RNA modifying enzymes and emerging regulators of gene expression? RNA biology 14, 1185–1196 (2017). [PubMed: 28045575]
10. Carlile TM, et al. Pseudouridine profiling reveals regulated mRNA pseudouridylation in yeast and human cells. Nature 515, 143–146 (2014). [PubMed: 25192136]
11. Li X, et al. Chemical pulldown reveals dynamic pseudouridylation of the mammalian transcriptome. Nature chemical biology 11, 592–597 (2015). [PubMed: 26075521]
12. Schwartz S, et al. Transcriptome-wide mapping reveals widespread dynamic-regulated pseudouridylation of ncRNA and mRNA. Cell 159, 148–162 (2014). [PubMed: 25219674]
13. Lovejoy AF, Riordan DP & Brown PO Transcriptome-wide mapping of pseudouridines: pseudouridine synthases modify specific mRNAs in S. cerevisiae. PloS one 9, e110799 (2014).
14. Song J, et al. Differential roles of human PUS10 in miRNA processing and tRNA pseudouridylation. Nature chemical biology 16, 160–169 (2020). [PubMed: 31819270]
15. Lei Z. & Yi C. A Radiolabeling-Free, qPCR-Based Method for Locus-Specific Pseudouridine Detection. Angew Chem Int Ed Engl 56, 14878–14882 (2017). [PubMed: 28960747]
16. Guzzi N, et al. Pseudouridylation of tRNA-Derived Fragments Steers Translational Control in Stem Cells. Cell 173, 1204–1216 e1226 (2018). [PubMed: 29628141]
17. Penzo M, Guerrieri AN, Zacchini F, Trere D. & Montanaro L. RNA Pseudouridylation in Physiology and Medicine: For Better and for Worse. Genes 8(2017).
18. Johnson DR & O'Neill BP Glioblastoma survival in the United States before and during the temozolomide era. Journal of neuro-oncology 107, 359–364 (2012). [PubMed: 22045118]
19. Stupp R, et al. Effects of radiotherapy with concomitant and adjuvant temozolomide versus radiotherapy alone on survival in glioblastoma in a randomised phase III study: 5-year analysis of the EORTC-NCIC trial. Lancet Oncol 10, 459–466 (2009). [PubMed: 19269895]
20. Cui Q, et al. Downregulation of TLX induces TET3 expression and inhibits glioblastoma stem cell self-renewal and tumorigenesis. Nature communications 7, 10637 (2016).
21. Shi Y, et al. Ibrutinib inactivates BMX-STAT3 in glioma stem cells to impair malignant growth and radioresistance. Science translational medicine 10(2018).
22. Man J, et al. Hypoxic Induction of Vasorin Regulates Notch1 Turnover to Maintain Glioma Stem-like Cells. Cell stem cell 22, 104–118 e106 (2018). [PubMed: 29198941]
23. Bao S, et al. Glioma stem cells promote radioresistance by preferential activation of the DNA damage response. Nature 444, 756–760 (2006). [PubMed: 17051156]
24. Duan S, et al. PTEN deficiency reprogrammes human neural stem cells towards a glioblastoma stem cell-like phenotype. Nature communications 6, 10068 (2015).
25. Sancho-Martinez I, et al. Establishment of human iPSC-based models for the study and targeting of glioma initiating cells. Nature communications 7, 10743 (2016).
26. Cui Q, et al. m6A RNA Methylation Regulates the Self-Renewal and Tumorigenesis of Glioblastoma Stem Cells. Cell reports 18, 2622–2634 (2017). [PubMed: 28297667]
27. Zhang S, et al. m(6)A Demethylase ALKBH5 Maintains Tumorigenicity of Glioblastoma Stem-like Cells by Sustaining FOXM1 Expression and Cell Proliferation Program. Cancer cell 31, 591–606 e596 (2017). [PubMed: 28344040]
28. Dixit D, et al. The RNA m6A Reader YTHDF2 Maintains Oncogene Expression and Is a Targetable Dependency in Glioblastoma Stem Cells. Cancer Discov 11, 480–499 (2021). [PubMed: 33023892]
29. Fang R, et al. EGFR/SRC/ERK-stabilized YTHDF2 promotes cholesterol dysregulation and invasive growth of glioblastoma. Nature communications 12, 177 (2021).

30. Waalkes TP, Dinsmore SR & Mrochek JE Urinary excretion by cancer patients of the nucleosides N-dimethylguanosine, 1-methylinosine, and pseudouridine. Journal of the National Cancer Institute 51, 271–274 (1973). [PubMed: 4720877]
31. Stockert JA, et al. Predictive value of pseudouridine in prostate cancer. Am J Clin Exp Urol 7, 262–272 (2019). [PubMed: 31511832]
32. Zhao Z, et al. Comprehensive RNA-seq transcriptomic profiling in the malignant progression of gliomas. Sci Data 4, 170024 (2017). [PubMed: 28291232]
33. Gusev Y, et al. The REMBRANDT study, a large collection of genomic data from brain cancer patients. Sci Data 5, 180158 (2018). [PubMed: 30106394]
34. Brennan CW, et al. The somatic genomic landscape of glioblastoma. Cell 155, 462–477 (2013). [PubMed: 24120142]
35. Gravendeel LA, et al. Intrinsic gene expression profiles of gliomas are a better predictor of survival than histology. Cancer research 69, 9065–9072 (2009). [PubMed: 19920198]
36. Cohen AL, Holmen SL & Colman H. IDH1 and IDH2 mutations in gliomas. Curr Neurol Neurosci Rep 13, 345 (2013). [PubMed: 23532369]
37. Labussiere M, et al. All the 1p19q codeleted gliomas are mutated on IDH1 or IDH2. Neurology 74, 1886–1890 (2010). [PubMed: 20427748]
38. Suva ML, et al. Reconstructing and reprogramming the tumor-propagating potential of glioblastoma stem-like cells. Cell 157, 580–594 (2014). [PubMed: 24726434]
39. Ligon KL, et al. Olig2-regulated lineage-restricted pathway controls replication competence in neural stem cells and malignant glioma. Neuron 53, 503–517 (2007). [PubMed: 17296553]
40. Veselska R, et al. Nestin expression in the cell lines derived from glioblastoma multiforme. BMC Cancer 6, 32 (2006). [PubMed: 16457706]
41. Anido J, et al. TGF-beta Receptor Inhibitors Target the CD44(high)/Id1(high) Glioma-Initiating Cell Population in Human Glioblastoma. Cancer cell 18, 655–668 (2010). [PubMed: 21156287]
42. Liu G, et al. Analysis of gene expression and chemoresistance of CD133+ cancer stem cells in glioblastoma. Molecular cancer 5, 67 (2006). [PubMed: 17140455]
43. Son MJ, Woolard K, Nam DH, Lee J. & Fine HA SSEA-1 is an enrichment marker for tumor-initiating cells in human glioblastoma. Cell stem cell 4, 440–452 (2009). [PubMed: 19427293]
44. Bao S, et al. Targeting cancer stem cells through L1CAM suppresses glioma growth. Cancer research 68, 6043–6048 (2008). [PubMed: 18676824]
45. Ogden AT, et al. Identification of A2B5+CD133- tumor-initiating cells in adult human gliomas. Neurosurgery 62, 505–514; discussion 514–505 (2008). [PubMed: 18382330]
46. Qiang L, et al. Isolation and characterization of cancer stem like cells in human glioblastoma cell lines. Cancer Lett 279, 13–21 (2009). [PubMed: 19232461]
47. Behm-Ansmant I, et al. The Saccharomyces cerevisiae U2 snRNA:pseudouridine-synthase Pus7p is a novel multisite-multisubstrate RNA:Psi-synthase also acting on tRNAs. RNA (New York, N.Y 9, 1371–1382 (2003).
48. Taoka M, et al. Landscape of the complete RNA chemical modifications in the human 80S ribosome. Nucleic acids research 46, 9289–9298 (2018). [PubMed: 30202881]
49. Seidel A, Brunner S, Seidel P, Fritz GI & Herbarth O. Modified nucleosides: an accurate tumour marker for clinical diagnosis of cancer, early detection and therapy control. British journal of cancer 94, 1726–1733 (2006). [PubMed: 16685264]
50. Frye M, Harada BT, Behm M. & He C. RNA modifications modulate gene expression during development. Science (New York, N.Y 361, 1346–1349 (2018).
51. Zheng LL, et al. tRF2Cancer: A web server to detect tRNA-derived small RNA fragments (tRFs) and their expression in multiple cancers. Nucleic acids research 44, W185–193 (2016). [PubMed: 27179031]
52. Pickerill ES, et al. Pseudouridine synthase 7 impacts Candida albicans rRNA processing and morphological plasticity. Yeast 36, 669–677 (2019). [PubMed: 31364194]
53. Darvish H, et al. A novel PUS7 mutation causes intellectual disability with autistic and aggressive behaviors. Neurol Genet 5, e356 (2019). [PubMed: 31583274]

54. de Brouwer APM, et al. Variants in PUS7 Cause Intellectual Disability with Speech Delay, Microcephaly, Short Stature, and Aggressive Behavior. Am J Hum Genet 103, 1045–1052 (2018). [PubMed: 30526862]
55. Silginer M, et al. Autocrine activation of the IFN signaling pathway may promote immune escape in glioblastoma. Neuro-oncology 19, 1338–1349 (2017). [PubMed: 28475775]
56. Zhan X, et al. Glioma stem-like cells evade interferon suppression through MBD3/NuRD complex-mediated STAT1 downregulation. J Exp Med 217(2020).
57. Alvarado AG, et al. Glioblastoma Cancer Stem Cells Evade Innate Immune Suppression of Self-Renewal through Reduced TLR4 Expression. Cell stem cell 20, 450–461 e454 (2017). [PubMed: 28089910]
58. Pencheva N, et al. Identification of a Druggable Pathway Controlling Glioblastoma Invasiveness. Cell reports 20, 48–60 (2017). [PubMed: 28683323]
59. Zhu Z, et al. Zika Virus Targets Glioblastoma Stem Cells through a SOX2-Integrin alphavbeta5 Axis. Cell stem cell 26, 187–204 e110 (2020). [PubMed: 31956038]
60. Shi Y, et al. Expression and function of orphan nuclear receptor TLX in adult neural stem cells. Nature 427, 78–83 (2004). [PubMed: 14702088]
61. Bowman RL, Wang Q, Carro A, Verhaak RG & Squatrito M. GlioVis data portal for visualization and analysis of brain tumor expression datasets. Neuro-oncology 19, 139–141 (2017). [PubMed: 28031383]
62. Hanzelmann S, Castelo R. & Guinney J. GSVA: gene set variation analysis for microarray and RNA-seq data. BMC Bioinformatics 14, 7 (2013). [PubMed: 23323831]
63. Su R, et al. Targeting FTO Suppresses Cancer Stem Cell Maintenance and Immune Evasion. Cancer cell 38, 79–96 e11 (2020). [PubMed: 32531268]
64. Van Nostrand EL, et al. Robust transcriptome-wide discovery of RNA-binding protein binding sites with enhanced CLIP (eCLIP). Nature methods 13, 508–514 (2016). [PubMed: 27018577]
65. Li X, et al. Base-Resolution Mapping Reveals Distinct m(1)A Methylome in Nuclear- and Mitochondrial-Encoded Transcripts. Molecular cell 68, 993–1005 e1009 (2017). [PubMed: 29107537]
66. Bailey TL, et al. MEME SUITE: tools for motif discovery and searching. Nucleic acids research 37, W202–208 (2009). [PubMed: 19458158]
67. Yu G, Wang LG, Han Y. & He QY clusterProfiler: an R package for comparing biological themes among gene clusters. OMICS 16, 284–287 (2012). [PubMed: 22455463]
68. Subramanian A, et al. Gene set enrichment analysis: a knowledge-based approach for interpreting genome-wide expression profiles. Proceedings of the National Academy of Sciences of the United States of America 102, 15545–15550 (2005). [PubMed: 16199517]
69. Mootha VK, et al. PGC-1alpha-responsive genes involved in oxidative phosphorylation are coordinately downregulated in human diabetes. Nature genetics 34, 267–273 (2003). [PubMed: 12808457]
70. Wang X, et al. N(6)-methyladenosine Modulates Messenger RNA Translation Efficiency. Cell 161, 1388–1399 (2015). [PubMed: 26046440]

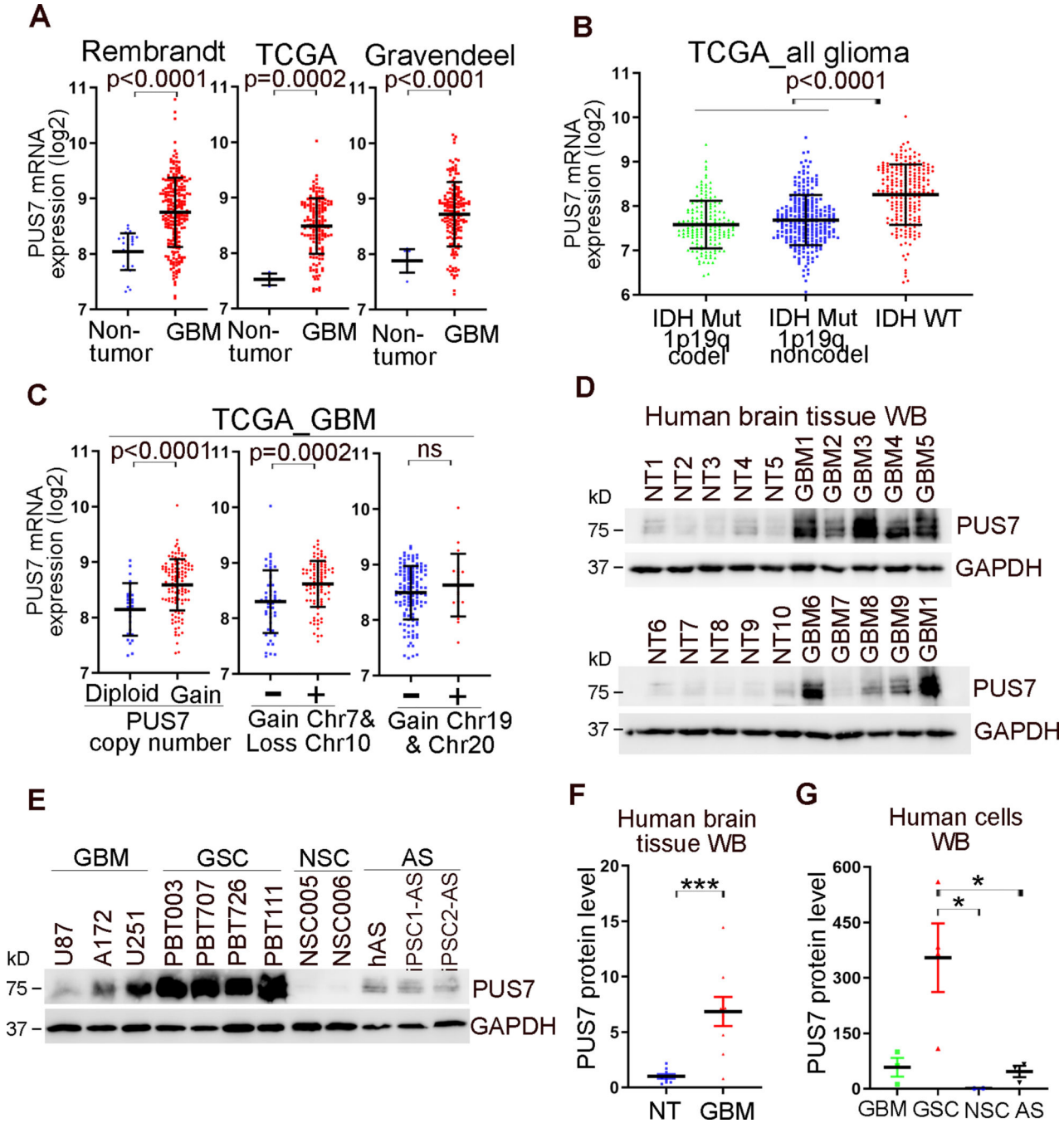

Figure 1. PUS7 is highly expressed in GBM patients.

(A) The expression of PUS7 in GBM patients and non-tumor control samples from the REMBRANDT (n=28 non-tumor samples and n=219 GBM samples), TCGA (n=4 non-tumor samples and n=156 GBM samples), and Gravendeel (n=8 non-tumor samples and n=159 GBM samples) datasets. **(B)** The expression of PUS7 in all glioma patients stratified by IDH mutation status and 1p19q chromosome co-deletion status from the TCGA dataset (n=169 IDH mut 1p19q codel patients, n=258 IDH mut 1p19q noncodel patients, n=229 IDH WT patients). (**C**) The expression of PUS7 in GBM patients stratified by the status

of PUS7 copy number variation (n=26 diploid patients and n=120 gain patients), gain of chromosome 7 and loss of chromosome 10 (n=50 patients for negative group and n=96 patients for positive group), or gain of chromosome 19 and 20 (n=127 patients for negative group and n=19 patients for positive group) in the TCGA dataset. (**D**) The expression of PUS7 in GBM patients and in non-tumor control samples analyzed by Western blot. The uncropped blot images for the cropped images shown here are in the source data. Repeated twice with similar results. (**E**) The expressions of PUS7 in GSCs, NSCs, established GBM lines, and astrocytes (hAS: primary human astrocytes; iPSC1-AS and iPSC2-AS: human iPSC-derived astrocytes) analyzed by Western blot. The uncropped blot images for the cropped images shown here are in the source data. Repeated twice with similar results. (**F**) Quantification of PUS7 expression in GBM patients and in non-tumor control samples analyzed by Western blot. n = 9 GBM patients and 10 non-tumor control subjects. p=0.0001. (**G**) Quantification of the expression level of PUS7 in 4 lines of GSCs, 2 lines of NSCs, 3 established GBM lines, and 3 lines of astrocytes analyzed by Western blot. Error bars are SD of the mean for **A-C**. p=0.0212 for GSCs vs NSCs, p=0.0226 for GSCs vs astrocytes. p value was determined by two-tailed Student's t-test for **A-C**. ns: not statistically significant (p=0.2626 for gain of chromosome 19 and 20 in **C**). Error bars represent SE of the mean for panels **F** and **G**. ***p<0.001 by one-tailed Student's t-test for panel **F**. *p<0.05 by One-way ANOVA and Dunnett's multiple comparisons test for panel **G**. See also Extended Data Figure 1.

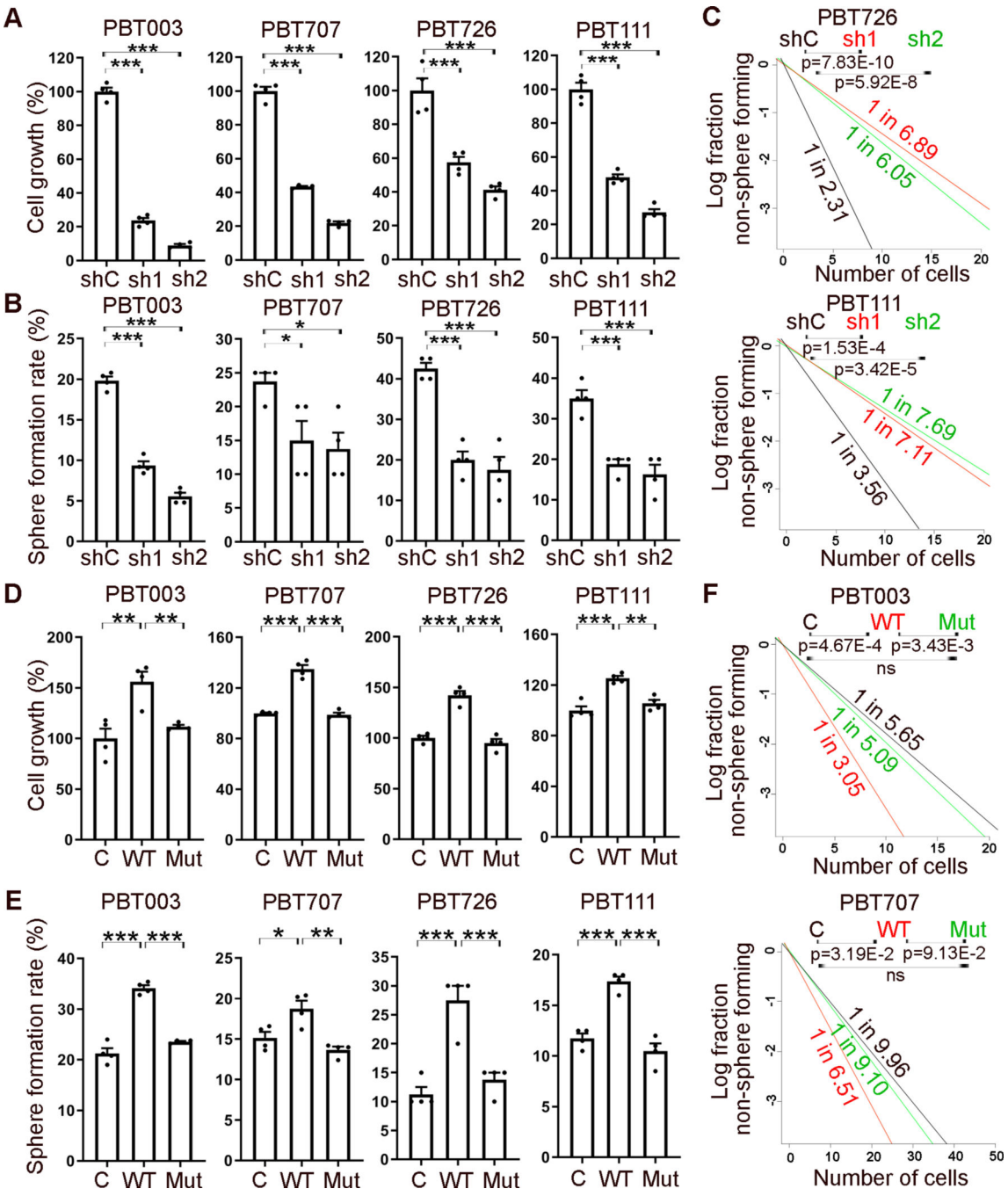

Figure 2. PUS7 regulates GSC growth and self-renewal.

(A) Cell growth of GSCs (PBT003, PBT707, PBT726, and PBT111) transduced with lentivirus expressing control shRNA (shC) or PUS7 shRNA (sh-1 and sh-2). n=4 cell culture replicates. p<0.0001 for PBT003, PBT707, and PBT111; p=0.0003 for PBT726-sh1, and p<0.0001 for PBT726-sh2. **(B)** Sphere formation of GSCs transduced with lentivirus expressing control shRNA (shC) or PUS7 shRNA (sh1 and sh2). n=4 cell culture replicates. p<0.0001 for PBT003; p=0.0428 for PBT707-sh1, p=0.0231 for PBT707-sh2; p=0.0002 for PBT726-sh1, p<0.0001 for PBT726-sh2; p=0.0005 for PBT111-sh1, and p=0.0002

for PBT111-sh2. **(C)** Limiting dilution assay (LDA) of GSCs transduced with lentivirus expressing control shRNA (shC) or PUS7 shRNA (sh1 and sh2). **(D)** The growth of GSCs transduced with lentivirus expressing the WT or the mutant PUS7. n=4 cell culture replicates. p=0.0015 for PBT003-C, p=0.0067 for PBT003-Mut; p<0.0001 for PBT707 and PBT726; p=0.0002 for PBT111-C, and p=0.0011 for PBT111-Mut. **(E)** Sphere formation of GSCs transduced with lentivirus expressing the WT or the mutant PUS7. n=4 cell culture replicates. p<0.0001 for PBT003; p=0.0145 for PBT707-C, p=0.0018 for PBT707-Mut; p=0.0002 for PBT726-C, p=0.0007 for PBT726-Mut; p=0.0001 for PBT111-C, and p<0.0001 for PBT111-Mut. **(F)** LDA of GSCs transduced with lentivirus expressing the WT or the mutant PUS7 controls. Error bars are SE of the mean for panels **A**, **B, D** and **E**. *p<0.05, **p<0.01, and ***p<0.001 by One-way ANOVA and Dunnett's multiple comparisons test for panels **A**, **B, D** and **E**. p value for the LDA assay in panels **C** and **F** was provided by the ELDA webtool analysis. See also Extended Data Figure 2 and 3.

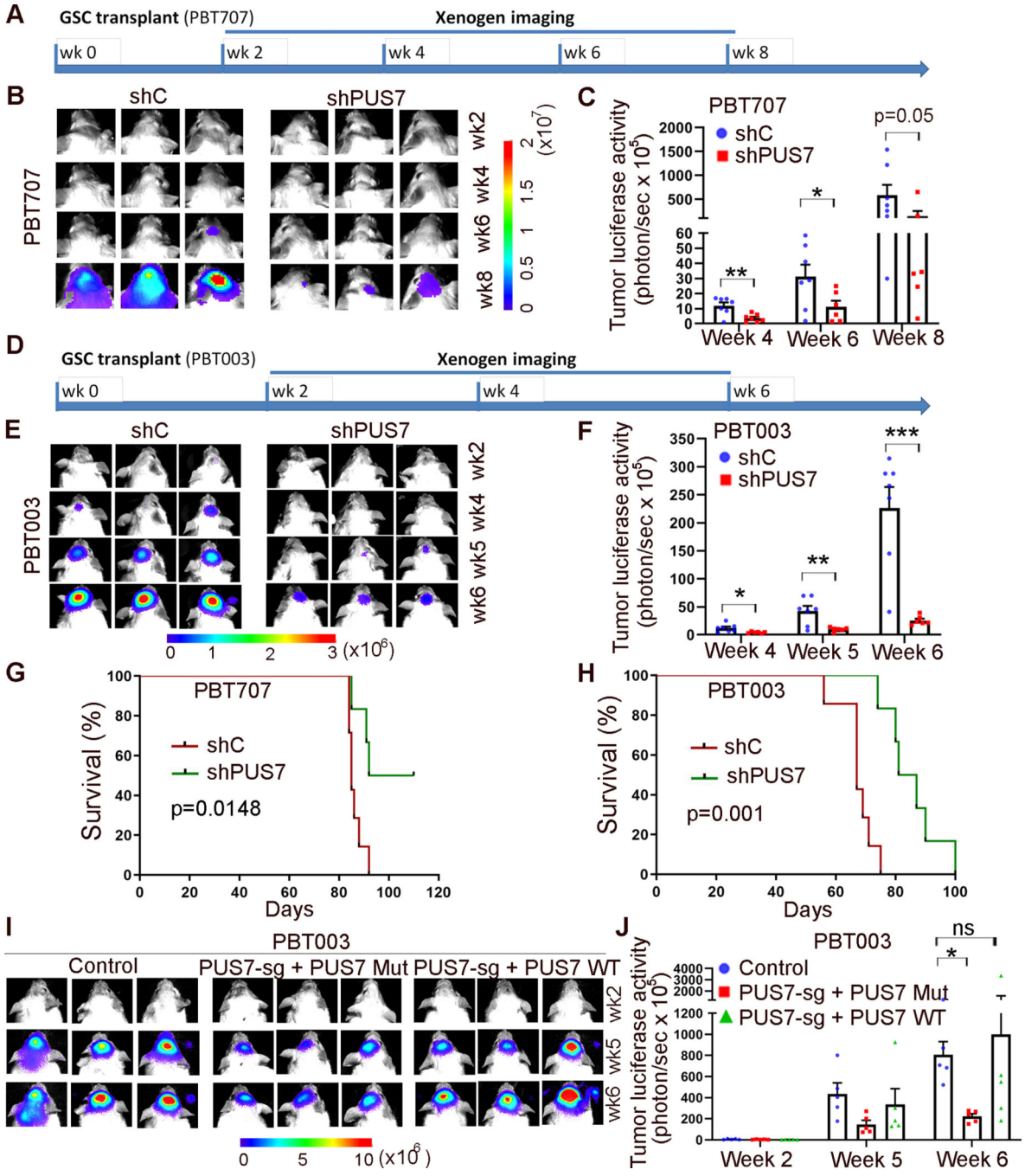

Figure 3. Reduction of PUS7 expression suppresses tumor progression.

(A) Schematic of the experimental design, including PBT707 GSC transplantation and bioluminescent imaging of xenografted tumors. **(B)** Bioluminescent images of brain tumors in NSG mice transplanted with PBT707 GSCs that were transduced with control shRNA (shC) or PUS7 shRNA (shPUS7). **(C)** Quantification of the bioluminescence intensity of tumors after PBT707 GSC transplantation. n=7 mice per group. p=0.0025 for week 4, p=0.0284 for week 6. **(D)** Schematic of the experimental design, including PBT003 GSC transplantation and bioluminescent imaging of xenografted tumors. **(E)** Bioluminescent

images of brain tumors in NSG mice transplanted with PBT003 GSCs that were transduced with shC or shPUS7. **(F)** Quantification of the bioluminescence intensity of tumors after PBT003 GSC transplantation. n=7 mice for shC control and n=6 mice for shPUS7 group. p=0.0124 for week 4, p=0.0039 for week 5, and p=0.0002 for week 6. **(G, H)** The survival curve of NSG mice transplanted with PBT707 GSCs (**G**) or PBT003 GSCs (**H**) transduced with shC or shPUS7. The X axis represents days after GSC transplantation. n=7 mice for shC control and n=6 mice for shPUS7 group for panels **G** and **H**. **(I)** Bioluminescent images of brain tumors in NSG mice transplanted with PBT003 GSCs transduced with control sgRNA, or PUS7 sgRNA (PUS7-sg) with the WT or mutant PUS7. **(J)** Quantification of the bioluminescence intensity of tumors after PBT003 GSC transplantation. n=5 mice per group. p=0.0141 for PUS7-sg + PUS7 Mut group and p=0.9293 (ns) for PUS7-sg + PUS7 WT group for week 6. *p<0.05 by two-way ANOVA and Dunnett's multiple comparisons test. Error bars are SE of the mean for panels **C, F** and **J**. *p<0.05, **p<0.01, and ***p<0.001 by one-tailed Student's t test for panels **C** and **F**. Log-rank test for panels **G** and **H**. See also Extended Data Figure 4.

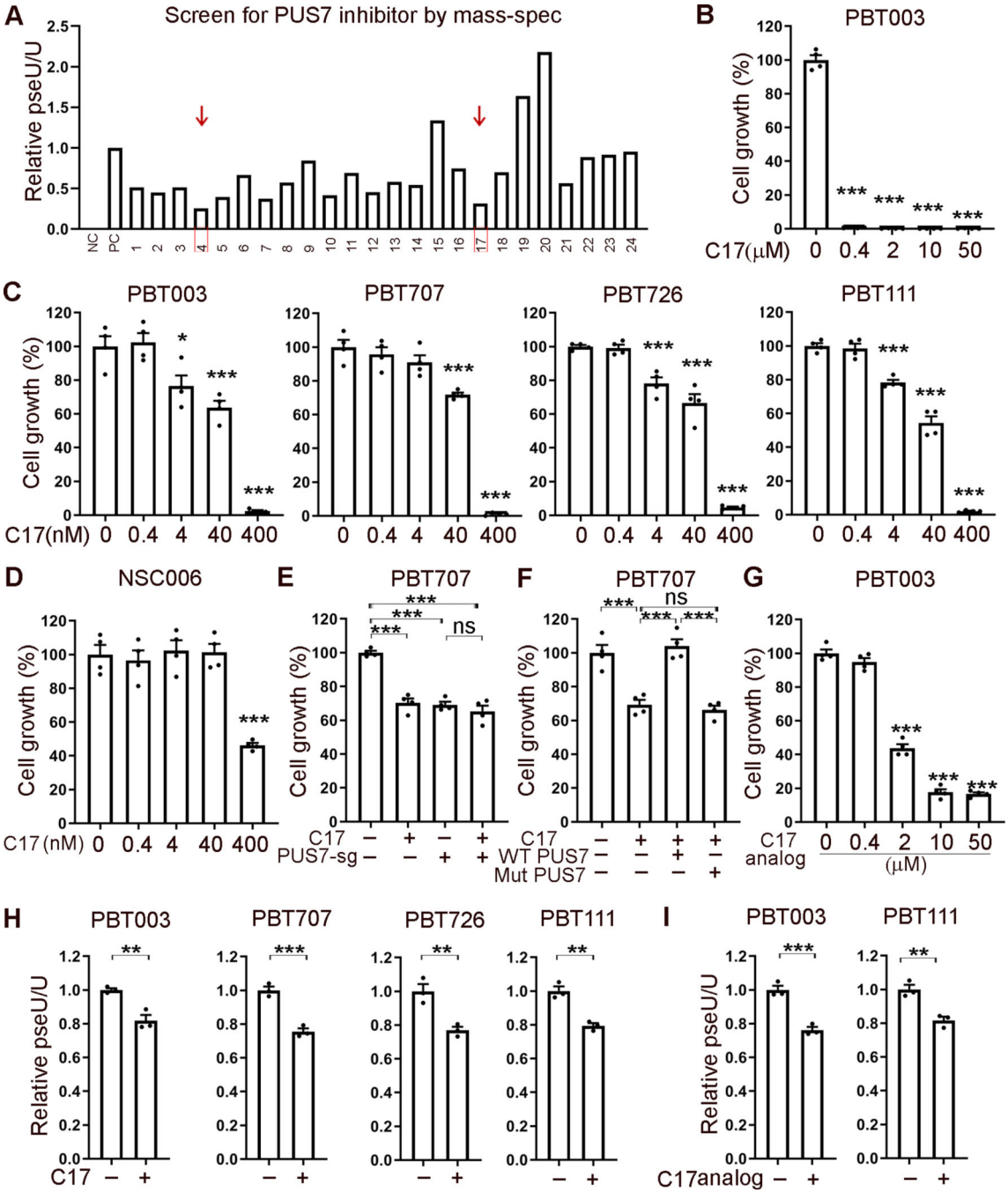

Figure 4. PUS7 inhibitors suppress GSC growth.

(A) Mass spectrometry (MS)-based PUS7 activity assay for screening PUS7 inhibitors. PseU: pseudouridine. **(B)** The dose effect of the C17 PUS7 inhibitor on the growth of PBT003 GSCs. A dose range of 0 to 50 μM was tested. n=4 cell culture replicates. $p<0.0001$ for all doses tested compared to 0 μM condition. **(C)** The effect of the C17 PUS7 inhibitor on the growth of multiple GSC lines (PBT003, PBT707, PBT726, and PBT111) in nM dose range. A dose range of 0 to 400 nM was tested. n=4 cell culture replicates. $p=0.0143$, 0.0004, and <0.0001 for 4, 40, and 400 nM conditions, respectively, in PBT003; $p=0.0001$,

<0.0001 for 40, 400 nM conditions, respectively, in PBT707; p=0.0005, <0.0001, <0.0001 for 4, 40, and 400 nM conditions, respectively, in PBT726; p<0.0001, <0.0001, and <0.0001 for 4, 40, and 400 nM conditions, respectively, in PBT111. **(D)** The effect of the C17 PUS7 inhibitor on the growth of NSC006 cells. n=4 cell culture replicates. p<0.0001 for 400 nM condition in NSC006. **(E)** The growth of PBT707 GSCs treated with the C17 compound and lentivirus expressing control sgRNA or sgRNA for PUS7. n=4 cell culture replicates. p<0.0001 for all conditions compared to C17 (−) and PUS7-sg (−) condition. ns: p=0.6619. **(F)** Rescue of the growth inhibitory effect of C17 by the WT but not the mutant PUS7. n=4 cell culture replicates. p=0.0004 for C17 (−) and PUS7(−) vs C17 (+) and PUS7(−), p=0.0001 for C17 (+) and PUS7 (−) vs C17 (+) and WT PUS7 (+), p=0.9383 for C17 (+) and PUS7 (−) vs C17 (+) and Mut PUS7 (+), p<0.0001 for C17 (+) and WT PUS7 (+) vs C17 (+) and Mut PUS7 (+). **(G)** The dose effect of the C17 analog on the growth of PBT003 GSCs. n=4 cell culture replicates. p<0.0001 for 2, 10, and 50 μM conditions. **(H)** Pseudouridine levels in GSCs treated by C17 measured by MS. n=3 RNA sample replicates. p=0.0035 for PBT003, p=0.0006 for PBT707, p=0.0042 for PBT726, and p=0.0014 for PBT111. **(I)** Pseudouridine levels in GSCs treated by the C17 analog measured by MS. n=3 RNA sample replicates. p=0.0008 for PBT003 and p=0.0032 for PBT111. Error bars are SE of the mean. *p<0.05, **p<0.01, and ***p<0.001 by One-way ANOVA and Dunnett's multiple comparisons test for panels **B-D** and **G,** by One-way ANOVA and Tukey's multiple comparisons test for panels **E-F**, by one-tailed Student's t test for panels **H** and **I**. See also Extended Data Figure 5.

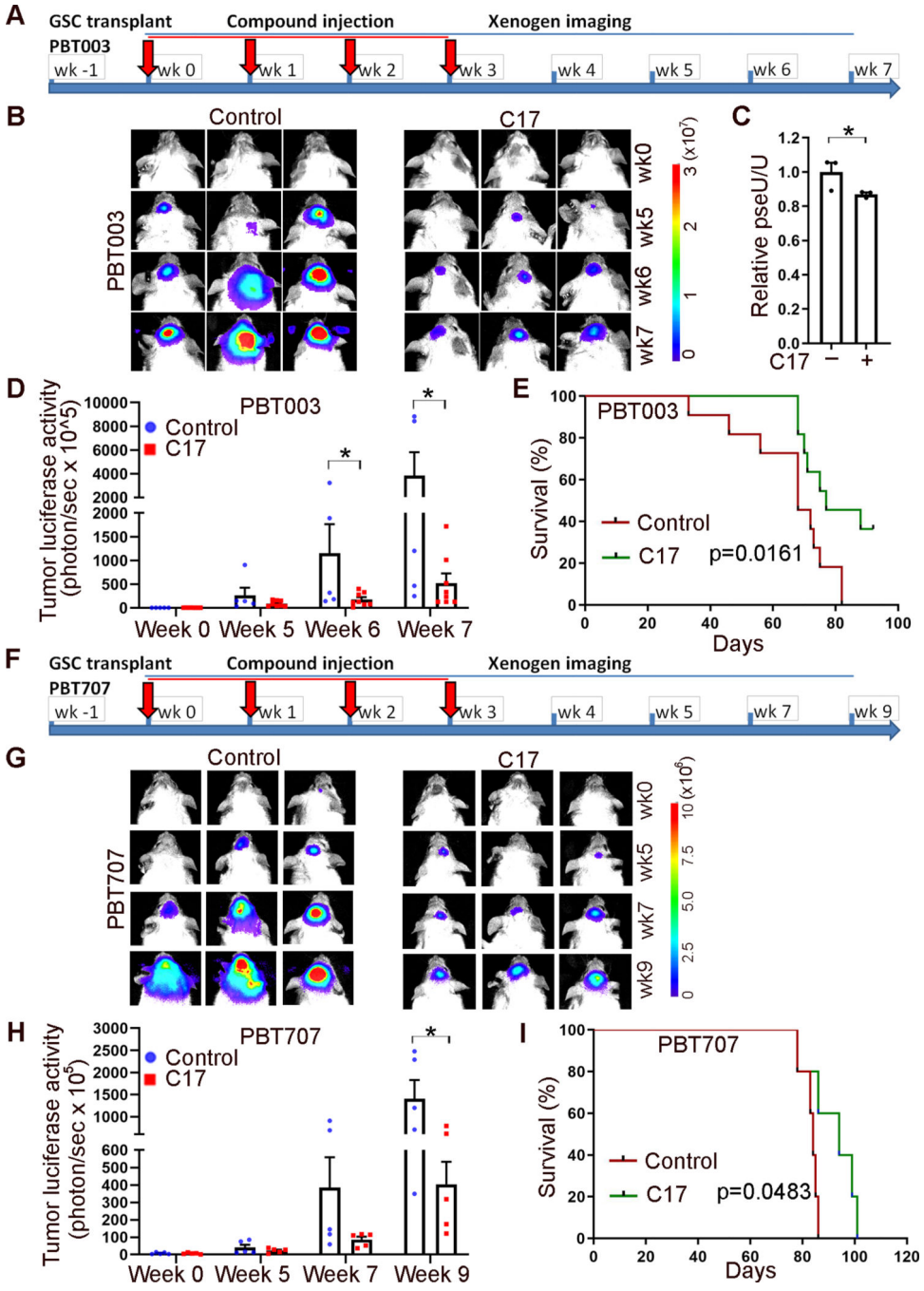

Figure 5. The PUS7 inhibitor suppresses tumor progression.

(A) Schematic of the experimental design, including PBT003 GSC transplantation, C17 compound treatment, and bioluminescent imaging of xenografted tumors. **(B)** Bioluminescent images of brain tumors in NSG mice treated with the C17 compound or vehicle control. **(C)** Quantification of the bioluminescence intensity of tumors in NSG mice treated with C17 or vehicle control. n=5 mice for control and n=8 mice for the C17 group. p=0.0323 for week 6 and p=0.0269 for week 7. **(D)** Pseudouridine levels in GSC-derived tumors treated by C17 measured by MS. n=3 RNA sample replicates. p=0.0398. **(E)** The

survival curve of NSG mice treated with C17 or vehicle control. The X axis represents days after treatment. n=11 mice per group. **(F)** Schematic of the experimental design, including PBT707 GSC transplantation, C17 compound treatment, and bioluminescent imaging of xenografted tumors. **(G)** Bioluminescent images of brain tumors in NSG mice treated with vehicle control or the C17 compound. **(H)** Quantification of the bioluminescence intensity of tumors in NSG mice treated with vehicle control or the C17 compound. n=5 mice per group. p=0.0267 for week 9. **(I)** The survival curve of NSG mice treated with vehicle control or the C17 compound. The X axis represents days after treatment. n=5 mice per group. Error bars are SE of the mean for panels **C, D** and **H**. *p<0.05 by one-tailed Student's t test for panels **C, D** and **H**. Log-rank test for panels **E** and **I**.

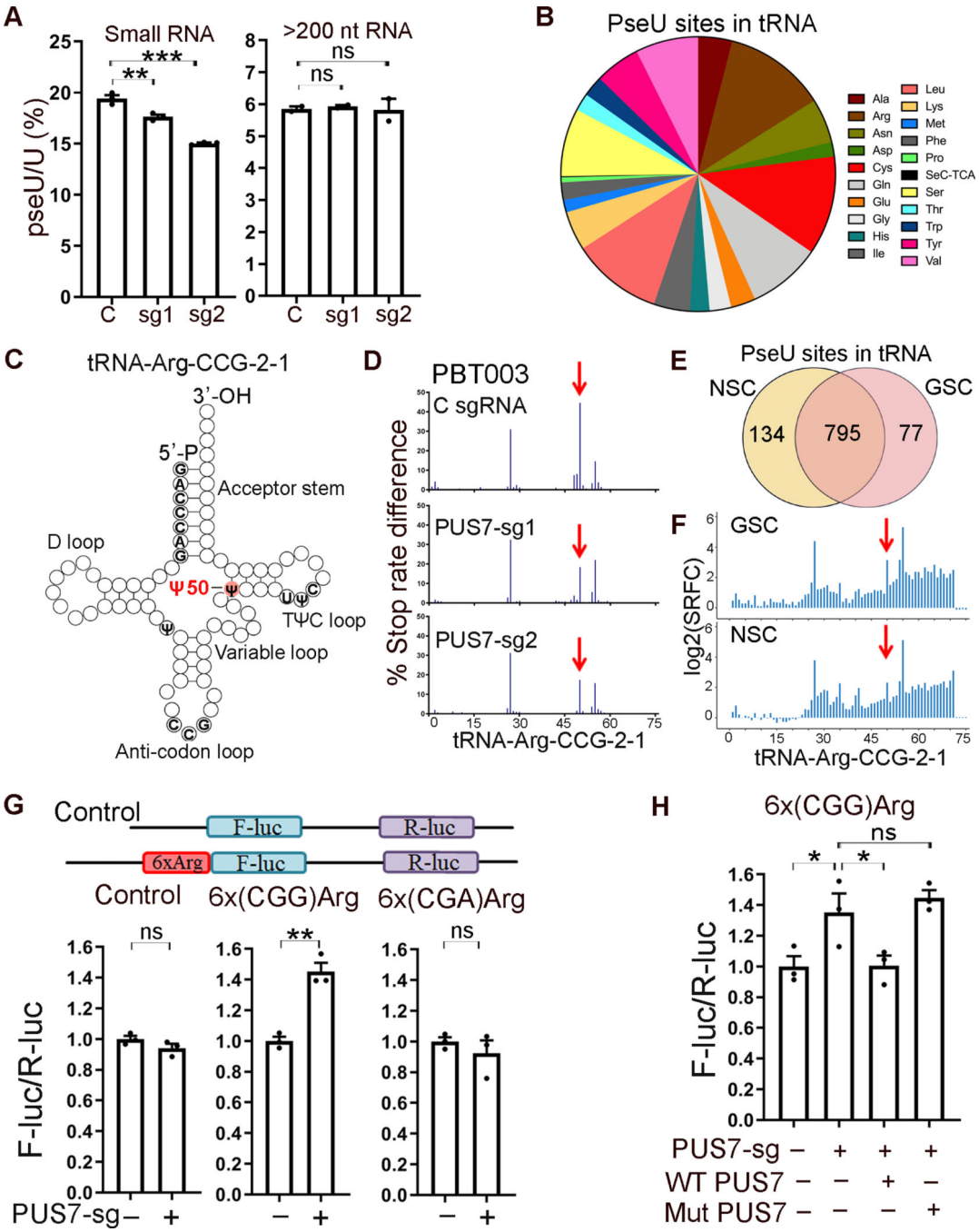

Figure 6. Pseudouridine modification profile in small RNAs.

(A) The pseudouridine (pseU) levels in small RNAs and >200 nt RNAs in PBT003 GSCs transduced with lentivirus expressing Cas9 and control sgRNA (C) or PUS7 sgRNA (sg1 and sg2). n=3 RNA sample replicates. p=0.0025 for sg1 and p<0.0001 for sg2. **(B)** Pseudouridine (PseU) sites in tRNAs in GSCs. ns: p=0.9341 for sg1 and p=0.966 for sg2. **(C)** Schematics of tRNA-Arg-CCG showing pseudouridine sites Ψ 27, Ψ 55 and PUS7-dependent pseudouridine site Ψ 50 (red). **(D)** A representative PUS7-dependent pseudouridine site identified by small RNA DM-Ψ-seq in GSCs. **(E)** PseU sites in tRNAs

in GSCs and NSCs. **(F)** A representative PUS7-dependent pseudouridine site in GSCs compared to NSCs. **(G)** KO of PUS7 induces Arg (CGG) codon-dependent increase of translation revealed by firefly luciferase (F-luc) assay. Renilla luciferase (R-luc) was included as a normalization control. n=3 cell culture replicates. p=0.0852 (ns) for control, p=0.0011 for 6x(CGG)Arg, and p=0.2183 (ns) for 6x(CGA)Arg. **(H)** The WT but not the mutant (mut) PUS7 could reverse PUS KO-induced Arg (CGG) codon-dependent translation. n=3 cell culture replicates. p=0.0379 for PUS7 sg (−) and PUS7 (−) vs PUS7 sg (+) and PUS7 (−), p=0.0415 for PUS7 sg (+) and PUS7 (−) vs PUS7 sg (+) and WT PUS7 (+), and p=0.762 (ns) for PUS7 sg (+) and PUS7 (−) vs PUS7 sg (+) and Mut PUS7 (+). Error bars are SE of the mean for panels **A**,**G**, and **H**. *p<0.05, **p<0.01, and ***p<0.001, and ns: not statistically significant (p>0.05) by One-way ANOVA and Dunnett's multiple comparisons test for panels **A** and **H**, by one-tailed Student's t test for panel **G**. See also Extended Data Figure 6.

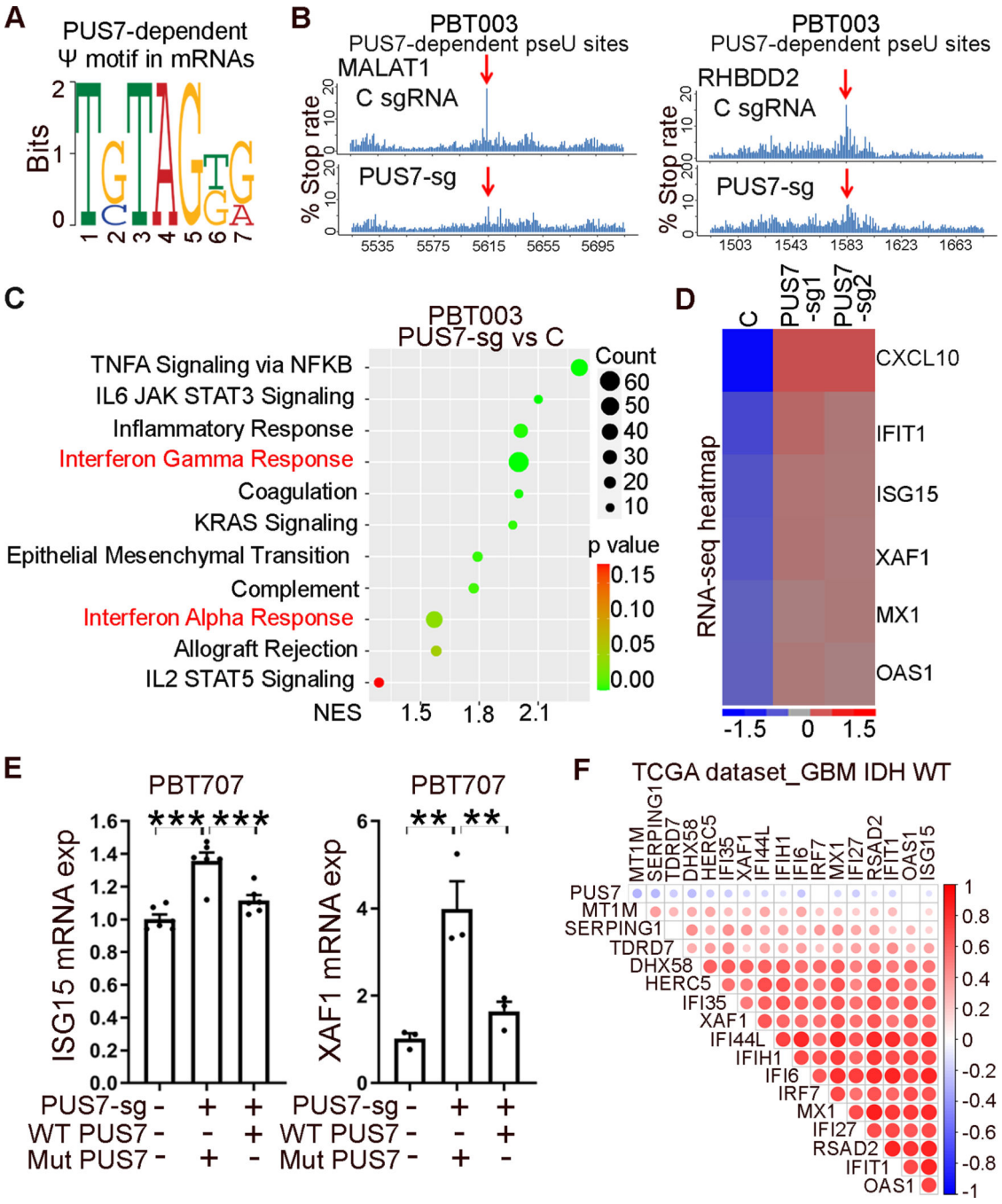

Figure 7. PUS7 regulates IFN pathway in GSC.

(**A**) A putative motif for PUS7-dependent pseudouridine sites in mRNAs in PBT003 GSCs. **(B)** Representative PUS7-dependent pseudouridine sites identified in mRNAs in PBT003 GSCs. **(C)** Gene set enrichment analysis of hallmark pathways enriched in PUS7 KO PBT003 GSCs from RNA-seq. **(D)** Heatmap showing ISG mRNA expression level change in PUS7 KO PBT003 GSCs. **(E)** RT-PCR of ISGs in PUS7 KO PBT707 cells with overexpression of the WT or the mutant PUS7. n=6 technical replicates for ISG15 and n=3 technical replicates for XAF1. p<0.0001 for PUS7 sg (−) and PUS7 (−) vs PUS7 sg (+) and

Mut PUS7 (+), p=0.0009 for PUS7 sg (+) and WT PUS7 (+) vs PUS7 sg (+) and Mut PUS7 (+) for ISG15; p=0.0031 for PUS7 sg (−) and PUS7 (−) vs PUS7 sg (+) and Mut PUS7 (+), and p=0.0098 for PUS7 sg (+) and WT PUS7 (+) vs PUS7 sg (+) and Mut PUS7 (+) for XAF1. Error bars are SE of the mean. **p<0.01 and ***p<0.001 by One-way ANOVA and Dunnett's multiple comparisons. **(F)** Correlation analysis of PUS7 expression and ISG gene expression in GBM IDH WT patients from the TCGA dataset. The degree of correlation was indicated by the size and color of the dots with bigger dots of higher intensity indicating a higher degree of correlation. Wells with dots indicate a significant (p<0.05) correlation, whereas blank wells indicate a non-significant (p>0.05) correlation. See also Extended Data Figure 7.

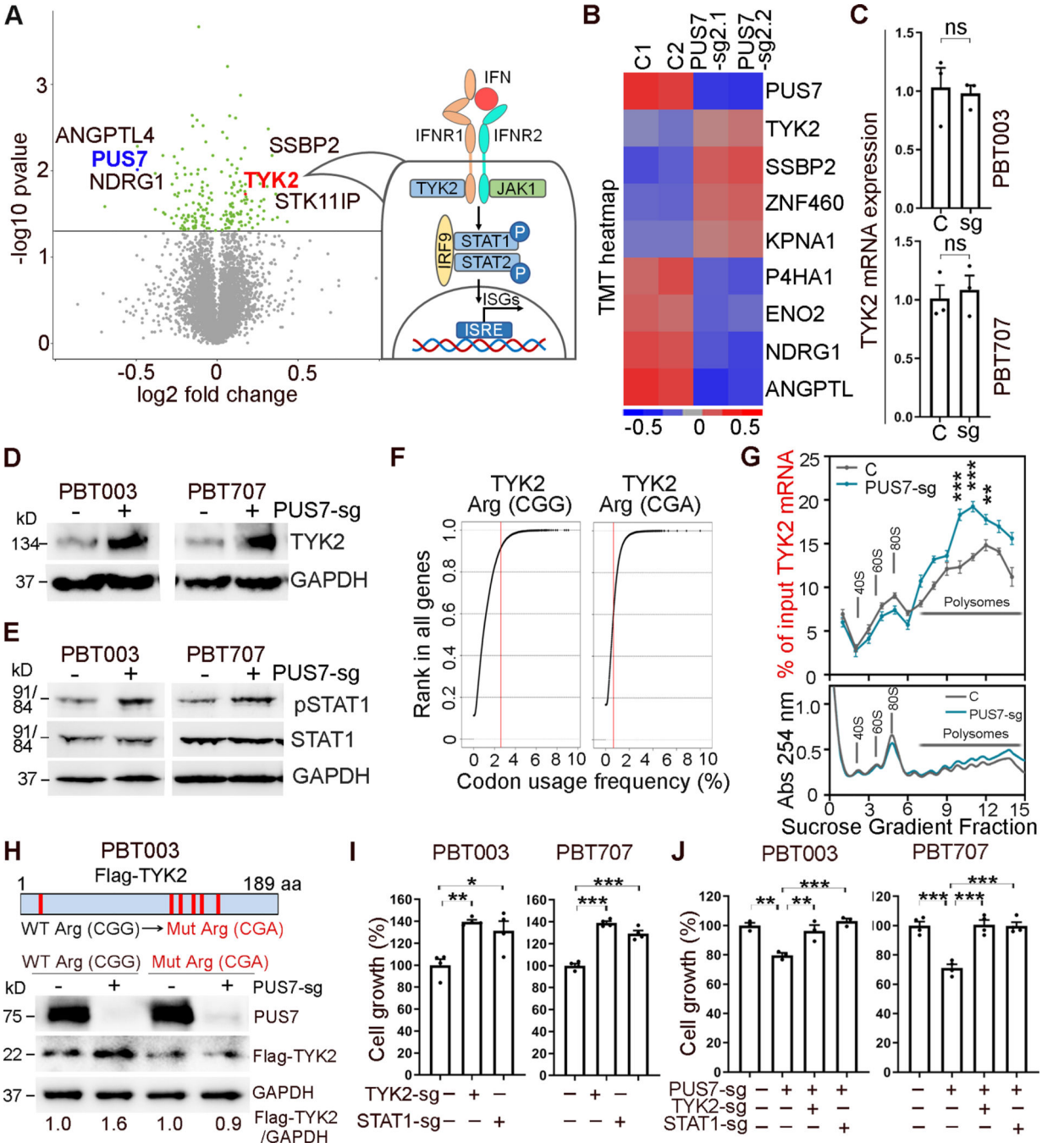

Figure 8. PUS7 regulates GSC growth through controlling TYK2-mediated IFN pathway.

(A) TMT mass spectrometry analysis of gene expression change at the protein level in PUS7 KO PBT003 GSCs. TYK2 (red dot), a regulator of IFN pathway, was up-regulated in PUS7 (blue dot) KO PBT003 GSCs, among significantly changed proteins (green dots). The IFN-TYK2 pathway was illustrated on the right. **(B)** Heatmap showing TMT mass spectrometry analysis of gene expression change at the protein level in PUS7 KO PBT003 GSCs. **(C)** RT-PCR of TYK2 in PUS7 KO GSCs. n=3 technical replicates. ns: not statistically significant (p=0.3967 for PBT003 and p=0.3445 for PBT707) by one-tailed

Student's t test. **(D)** Western blot of TYK2 in PUS7 KO GSCs. The uncropped blot images for the cropped images shown here are in the source data. Repeated three times with similar results. **(E)** Western blot of STAT1 and phosphorylated STAT1 (pSTAT1) in PUS7 KO GSCs. The uncropped blot images for the cropped images shown here are in the source data. Repeated twice with similar results. **(F)** Codon bias analysis of tRNA usage for TYK2 gene. **(G)** Polysome profiling analysis for TYK2 in PUS7 KO PBT003 GSCs. n=3 technical replicates. p=0.000538, 0.000069, and 0.001196 for fractions 10, 11, 12 respectively. **(H)** Western blot of the Flag-tagged WT or mutant TYK2 fragment in PUS7 KO GSCs. The uncropped blot images for the cropped images shown here are in the source data. Repeated twice with similar results. **(I)** Cell growth of GSCs transduced with lentivirus expressing control sgRNA (−) or sgRNA for TYK2 (TYK2-sg) or STAT1 (STAT1-sg). n=4 cell culture replicates. p=0.0025 for TYK2-sg in PBT003, p=0.0101 for STAT1-sg in PBT003; p<0.0001 for TYK2-sg in PBT707, and <0.0001 for STAT1-sg in PBT707. **(J)** Cell growth of GSCs transduced with lentivirus expressing sgRNA for PUS7 and transduced with lentivirus expressing sgRNA for TYK2 or STAT1. n=3 cell culture replicates for PBT003, n=4 cell culture replicates for PBT707. p=0.0012 for PUS7 sg (−) vs PUS7 sg (+), p=0.004 for PUS7 sg (+) vs PUS7 sg (+) and TYK2 sg (+), p=0.0005 for PUS7 sg (+) vs PUS7 sg (+) and STAT1 sg (+) in PBT003. p<0.0001 for PUS7 sg (−) vs PUS7 sg (+), PUS7 sg (+) vs PUS7 sg (+) and TYK2 sg (+), and PUS7 sg (+) vs PUS7 sg (+) and STAT1 sg (+) in PBT707. Error bars are SE of the mean for panels **C, G, I,** and **J**. *p<0.05, **p<0.01, and ***p<0.001by One-way ANOVA and Dunnett's multiple comparisons test for **I** and **J**, by multiple Student's t test for panel **G**. See also Extended Data Figure 8.